Spring 5-2022

The Performance Assessment of a Small Lighter-Than-Air Vehicle for Earth Science Remote Sensing Missions

Maxwell F. Burtis

THE PERFORMANCE ASSESSMENT OF A SMALL LIGHTER-THAN-AIR VEHICLE FOR EARTH SCIENCE REMOTE SENSING MISSIONS

by

Maxwell F. Burtis

A Thesis Submitted in Partial Fulfillment
of the Requirements for a Degree with Honors
(Mechanical Engineering)

The Honors College

University of Maine

May 2022

Advisory Committee:

Wilhelm M. Friess, Associate Professor of Mechanical Engineering, Advisor
Seth Campbell, Assistant Professor of Earth and Climate Sciences
Andrew J. Goupee, Associate Professor of Mechanical Engineering
Olivier Putzeys, Lectuer of Mechanical Engineering
Sharon S. Tisher, Lecturer of Economics, Honors College

ABSTRACT

This summer, a lighter-than-air (LTA) drone was tested in Alaska to measure glacier bedrock fracture density and orientation. Five flights were made in low wind conditions, and the directional stability of the airship made it too challenging to control in flight to realistically acquire useful image sets. The directional stability of the airship, when compared to an actively stabilized consumer-grade quadcopter was inferior. Flight logs and GPS data from the GPS on the LTA drone were analyzed and a quantitative assessment of the observed instability was made. The yaw axis and pitch were analyzed, and the yaw axis instability was greater than the pitch axis instability. The source of this instability included the excessive sensitivity of the yaw thruster, and the inherent yaw instability of the blimp shape. An attempt was made to reduce the yaw instability by reducing the yaw motor size. The observed instability may have also resulted from external sources like wind gusts and the glacier microclimate. The analysis informed modifications of the LTA drone to make it more stable for glacier research, which were implemented and tested. The thrust output of the tail motor was reduced by 59%. This change was associated with a reduction in median heading variability of 47% between test flights before and after modification. The reduction was proven statistically significant at a 99% confidence interval. Also, recommendations for further modifications include the implementation of autonomous flight control and envelope optimization.

ACKNOWLEDGMENTS

I could not have completed this work without all the generous support that I received. I'd like to formally thank UMaine's Center for Undergraduate Research, the Maine Space Grant Consortium, UMaine's College of Engineering, UMaine's Department of Mechanical Engineering, the UMaine Honors College, the Charlie Slavin Research Fund, and the Thomas E. Lynch Honors Thesis Scholarship for their financial backing of my research. I'd also like to thank Maine Bound Adventure Center and the Climate Change Institute for the equipment they allowed me to borrow so I could traverse the Juneau Icefield safely. I relied heavily on the members of my thesis committee throughout my research. My advisor Dr. Wilhelm Friess was integral, lending me his LTA drone and providing me with methodological advice. Dr. Sharon Tisher and Trixie Betz offered revisions and edits to better my writing. Dr. Seth Campbell, let me borrow his research equipment, introduced me to the field of Earth and Climate Sciences, and supported my research while on the Juneau Icefield. Dr. Andrew Goupee and Dr. Olivier Putzeys offered technical recommendations, and Crosby Lab Manager Stephen Abbadessa lent me research materials and supported the construction and testing of the LTA drone. I greatly appreciate the time and energy that the Juneau Icefield Research Program staff put into the logistics of this research which included the transport of helium by helicopter, and the construction of a temporary garage to house the drone. Lastly, I'd like to acknowledge that I conducted this research in the homeland of the Tlingit and Haida Tribes, where issues of resource and land rights are ongoing and where the impacts of colonization are still present.

DATA AND CODE AVAILABILITY

The code that was used and the data that support the findings of this study are openly available in [github] at https://github.com/maxburtis/LTA_thesis, reference number [1]

TABLE OF CONTENTS

LIST OF FIGURES

INTRODUCTION

Earth Science setting

The purpose of this research was to test the feasibility of the use of a lighter-than-air (LTA) drone or blimp as a platform for Earth Science remote sensing. Remote sensing is any form of gathering data without touching the object of interest [2, p. 34]. Aerial platforms are often used for remote sensing missions because they can move rapidly over an area with a large field of view, allowing for the efficient collection of large amounts of data [3]. Image sets can be acquired quickly using aerial platforms where images are stitched together to create maps or models [3],[4]. Terrain can be mapped by stitching together and georeferencing two-dimensional images [3]. Three-dimensional models can be created using techniques like photogrammetry, or structure-from-motion (SfM)[3],[4].

Photogrammetry involves capturing images of an object from different viewpoints to gain information about the three-dimensional space that the object occupies [5]. Data from the location and orientation of the camera is used in addition to georeferenced points in the images called ground control points (GCPs) [3],[4]. This information is integrated using software like Agisoft Metashape [6], which finds common points between photos called tie points. These points are made into a georeferenced, three-dimensional point cloud. Images are then laid on top of the point cloud to create a three-dimensional orthoimage of the terrain [4]. A depth map is created to determine how far each point is away from the camera and the adjacent points. Next, a mesh is created by connecting the points with a planar surface [7]. Finally, texture is added, and an accurate 3D model is created. This accuracy depends on the accuracy of the GPS used to

georeference the camera and GCPs, the resolution of the images that are collected, and the number of tie points that are found [8],[4],[3]. This technology is used by companies like Google to generate three-dimensional models of cities for Google Maps [9], but it is also useful for Earth scientists.

Earth scientists can use photogrammetry to map the Earth's surface features (glaciers, snow, ice, vegetation, water, bedrock, and surficial material) and the properties of each of these materials [4],[7],[3]. Photogrammetry can also be used to study processes that alter the Earth's surface, including, erosion, deposition, glacier advance and retreat, and the natural succession of vegetation [10],[4],[7],[3]. These processes involve changes that can be quantified through differencing repeat three-dimensional models. For example, a photogrammetry survey could be completed across a glacier one year, and then re-surveyed again five years later to quantify glacier volume change that comes from glacier advance or retreat [11]. The resulting models allow for the study of three-dimensional characteristics like volume change, whereas a two-dimensional representation would only determine a change in area [10],[11]. A three-dimensional model can demonstrate how much ice has melted and help inform predictions on sea-level rise [12], [13], changing down-glacier water resources, and impacts on associated ecosystems [14]. Changes in the Earth's crust can be linked to a changing climate [12],[13], and thus techniques like photogrammetry allows scientists to better model how a warming climate affects Earth system processes.

Southeast Alaska is a prime area to study the effects of global warming because the region is undergoing environmental rapid change [15],[16]. While there are many glaciers in Alaska, this work focused on the Juneau Icefield, a collection of glaciers north

of the state's capital. In 2016, the Juneau Icefield covered about 3700 km^2 in the northern Coast Mountains on the border between Alaska and British Colombia [17]. A map depicting the location of the Juneau Icefield is presented in [17, Fig. 1].

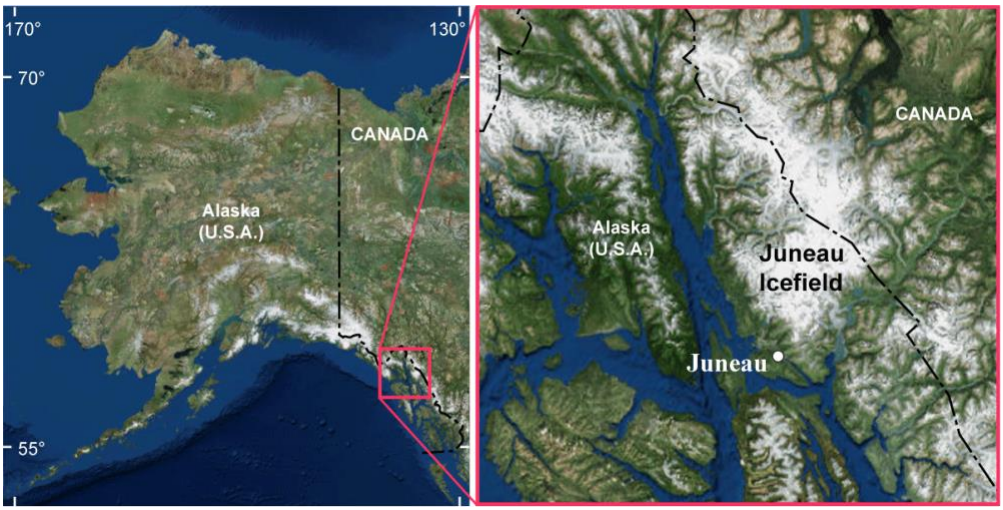

Fig. 1. The location of the Juneau Icefield. [18]

Historically, glaciers reached or nearly reached their current positions during the start of the Holocene. During the middle Holocene, glaciers advanced substantially, and in the last two centuries, they retreated rapidly [19]. Due to expected anthropogenic warming, the Juneau Icefield is predicted to lose two-thirds of its volume and area by the end of the century [17]. The largest glacier on the Juneau Icefield, the Taku Glacier, has been in retreat since 2013 [20]. In recent years, Alaskan glaciers have been melting at a faster rate than all other glaciated regions in the world which may be contributing to global sea-level rise, local water scarcity issues, and effects on local ecosystems [21],[14]. Because of the rapid changes occurring in Southeast Alaska, and the potential for these changes to impact the rest of the world, these changes must be studied so that better models and predictions can be made.

While the effects of global sea-level rise can be seen around the world, the changing climate is also responsible for regional effects. Glaciers profoundly impact the region through erosion. Fast-moving glaciers like the those found in Southeast Alaska are capable of eroding 10mm of bedrock per year [22]. Eroded material, or glacial till, impacts the chemistry and ecology of coastal Alaska because of the tight link between the ocean and the glacial runoff. Ground-up pieces of rock are carried downstream and induce changes to river and stream flow, biogeochemistry, local oceanography, and marine plants and animals [14]. Changing temperatures, precipitation, and subglacial hydrology all impact erosion rate. A rapidly changing climate may alter these variables and change erosion type and rate. Erosion rate will affect how much till is deposited downstream per unit time. Commonly used glacier erosion rate models approximate erosion rate E using the relationship established in [22, eq. (1)]:

$$E = K_g U_S^l \tag{1}$$

Where K_g is the bedrock erodibility constant, U_s is the glacier sliding velocity, and l is an exponent between one and four that depends on K_g. The erodibility constant is a measure of bedrock strength that depends on a variety of factors. Bedrock lithology, fracture density, and orientation all may vary spatially and affect how bedrock erodes [23],[24],[25]. Unfortunately, current bedrock erosion models are limited in their accuracy [26]. This is in part because K_g is often held constant despite spatial variations in bedrock strength [27],[22]. Common models don't account for spatial variations in lithology, fracture density, and orientation [23],[25]. Incorporating these properties into erosion models could result in more accurate predictions of erosion rate, which has

recently shown promise in the case of fracture density and orientation and could be a way to quantify erosion rates more realistically [28],[29],[30].

Measuring bedrock fracture density and orientation was the principal mission associated with this research on aerial sensing platforms. Granodiorite is the dominant lithology in the region and was constant throughout the test site [31]. This consistency allowed variations on erodibility to be constrained to bedrock fracture density and orientation. When a glacier flows parallel to the bedrock fractures, small grains of rock are eroded [23] which causes more turbid waters downstream. More turbid waters do not allow the sun's rays to penetrate the water's depths which may hinder the growth of photosynthetic plants [14]. When a glacier flows perpendicular to the bedrock fractures, the glacier will pluck away larger pieces of bedrock [23], which will result in less turbid waters downstream [14]. These effects of bedrock fracture density are illustrated below in [32, Fig. 2]. In areas of high bedrock fracture density, the bedrock is weaker, the erosion rate is faster, and more till is deposited downstream. In areas of low fracture density, the bedrock is stronger. Therefore, the erosion rate is slower, and less till is deposited downstream [25]. Understanding the amount and type of erosion will help researchers better understand how natural resources may be impacted. For example, the minerals and nutrients in glacial till can cause phytoplankton blooms that affect important fisheries like wild Pacific Salmon *(Oncorhynchus spp.)[14]*.

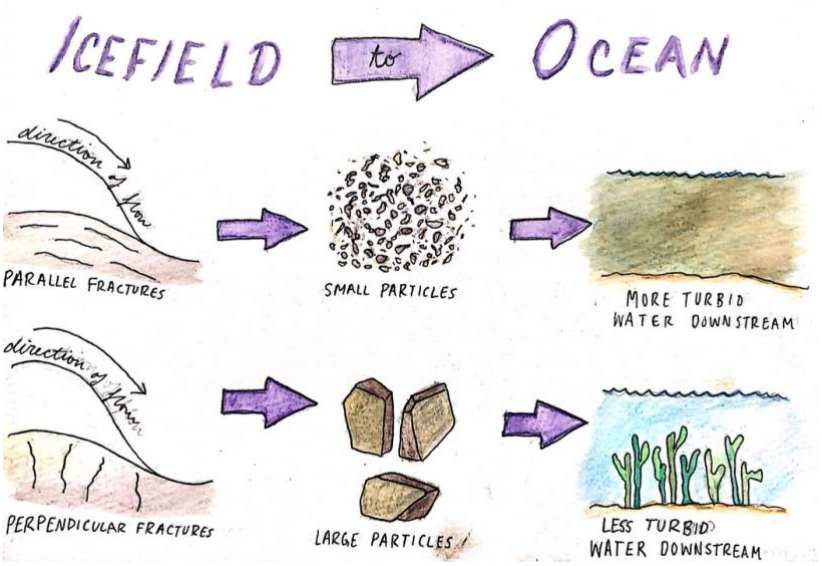

Fig. 2. Diagram of the effects of glacial till on downstream ecosystems. [32]

Photogrammetry was used from July-August of 2021 to develop orthorectified models of bedrock outcroppings that were then processed to quantify the bedrock fracture density and orientation. This was a continuation of work started by Colby Rand, a UMaine Honors College student who graduated in 2020 [33], and the project will be passed down and continued by future participants in the Juneau Icefield Research Program (JIRP). Drone images were collected using a DJI Phantom 4 Pro+ quadcopter and georeferenced using Elmid Reach RTK GPS units, and models were constructed using the photogrammetry software Agisoft Metashape. These models had an accuracy of up to 4.1 cm root-mean-square error. These models were flattened into an orthorectified mosaic and were processed using Laplacian edge detection algorithms in the photo processing software GIMP. Fracture density and orientation were then quantified in MATLAB to create the plots shown in Fig. 3. These plots have not yet been ground-truthed, which will be completed by future JIRP participants. This project is by no means complete, but the end goal of this work is to improve current surface geomorphological and glacier erosion models.

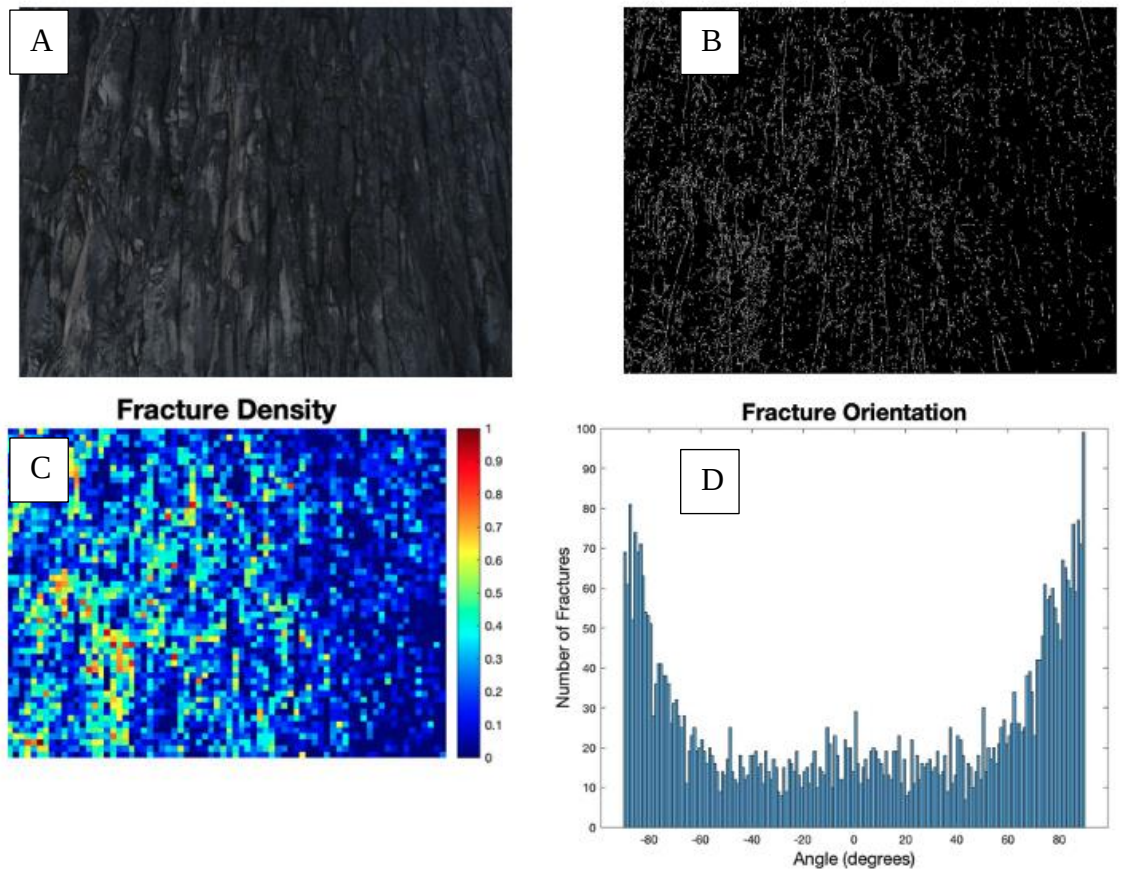

Fig. 3. The quantification of bedrock fracture density and orientation. A) Orthorectified image of bedrock outcropping. B) Laplacian edge detection algorithm applied to locate cracks. C) Plot of fracture density. D) Plot of fracture orientation.

Engineering setting

Drones have played a key role in the remote sensing industry. When compared to manned aircraft, unmanned aerial vehicles (UAVs) are often safer and cheaper. Because drones are unmanned, many of the risks associated with aircraft crashes can be avoided. Drones provide remote sensing in areas that are difficult or dangerous to access. For example, after the nuclear power plant in Fukushima, Japan suffered a catastrophic meltdown in March 2011, drones were used to inspect the damage because humans could have been hurt by the radiation [34]. Also, inspecting the underside of bridges is an expensive and time-consuming process, but drones are proving to make this process much cheaper and more efficient [35]. A single photogrammetry mapping flight using a

manned aircraft can cost upwards of $5,000 [36],[37] while a DJI Phantom 4 Pro+ quadcopter drone like the one used in this project retails for $2,039 [38]. The role of drones in remote sensing applications is becoming increasingly important as the UAV technology sector is developing fast. The past decade has witnessed a rapid expansion in the availability, capability, and popularity of small drones [39]. A report issued in 2019 by the Federal Aviation Administration predicts that the consumer and commercial UAV markets are growing faster than anticipated and could triple by 2023 [40]. The global commercial use of drones is estimated to have enabled over $127 billion in solutions in a variety of industries [41]. This explosion in drone use is supported by an ecosystem of software developers, integrators, and component manufacturers [42]. As seen in [43, Fig. 4,] growth is occurring across prosumer, recreational, and photogrammetry sectors.

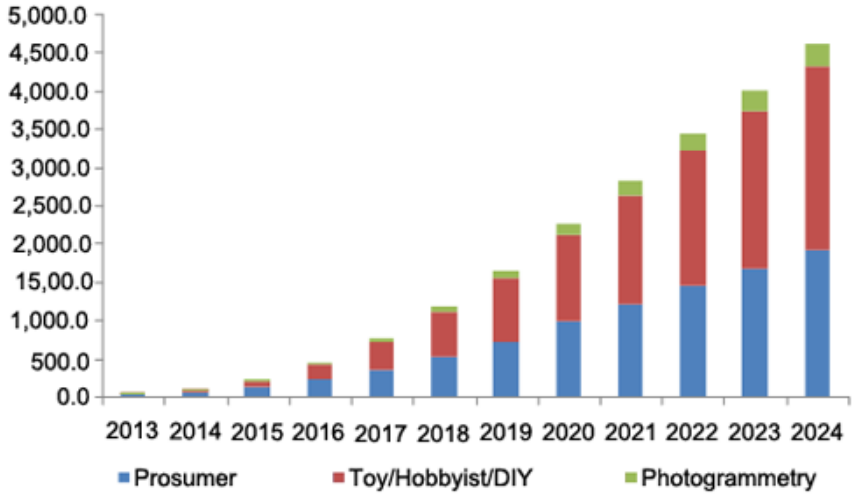

Fig. 4. North America consumer drone market by technology, 2012 - 2022 (USD Million). [43]

Fig. 5. Different types of common drones. A) Fixed-wing [45]. B) Multicopter (DJI Phantom 4 Pro+) [46]. C) Hybrid [47].

Despite the widespread adoption of drones, there are still some restrictions that limit the use of drones in many applications. Drones are commonly constrained by endurance, range, and payload. Payload is how much weight a drone can carry and is determined by how much lift that the drone can generate. The range is the total distance that a drone can fly, and endurance is how long the drone can fly on one battery. Both range and endurance are dependent on the size of the battery, the energy density of that battery, and how efficiently the drone can convert power into forward motion in the case of range or lift in the case of endurance. Common types of drones include multicopters, fixed-wings, and hybrids [40],[44] and are pictured in [45-47, Fig. 5]. In multicopters, the lift is generated by a set of motors with propellers. In fixed-wings, the lift is generated by a wing with an airfoil cross-section [44],[40],[48]. Fixed-wing drones tend to have longer endurance because they use less power to generate lift [44],[40]. The wing creates lift aerodynamically by causing a pressure differential between the top side and bottom side [48]. Hybrid drones are a combination of both of these technologies and generate lift with wings and propellers [40].

The consumer-grade multicopter drone used in this research had an endurance of 25 minutes while a fixed-wing drone built for a similar mission had a flight time of 30 minutes [49]. However, a major advantage that multicopters have over fixed-wing drones in the context of photogrammetry is their ability to fly slowly to acquire more detailed image sets [3]. Furthermore, they can take off and land vertically, while fixed-wings need to be launched into the air by hand or by a catapult [49]. The amount of lift that a fixed-wing aircraft generates is proportional to the square of the velocity at which the plane is flying as demonstrated by [50, eq. (2)] :

$$L = (1/2)\, d\, v^2\, s\, CL \quad (2)$$

where L is the lift, d is the density of air, v is the velocity of the aircraft, s is the surface area of the wings, and CL is the coefficient of lift. If the velocity is too low, the fixed-wing drone will stall and will not generate lift. Alternatively, multicopter lift is not dependent on speed, rather the thrust generated by the motors, meaning they can fly slowly enough to capture the high-resolution imagery needed for generating detailed models [3],[40]. Resolution is a function of altitude, flight speed, and the camera used [51]. The highest resolution images come from drones flying at slowly at low altitudes. In the photogrammetry setting, flights performed at a 70 m altitude at 20 m/s produced a 10 cm spatial resolution [52]. In comparison, at 45 m and 3.4 m/s a 3.1 cm resolution was obtained with a similar camera [8].

However, high-resolution cameras are heavy. Multicopters are commonly used for photogrammetry as they can fly at a lower speed than fixed-wings while carrying heavy payloads. However, they are limited by endurance. As seen in [35, Fig. 6], multicopters currently on the market tend to have decreasing endurance with increasing payload. There is a gap in this plot in the high endurance and high payload, a gap that could be filled using LTA technology.

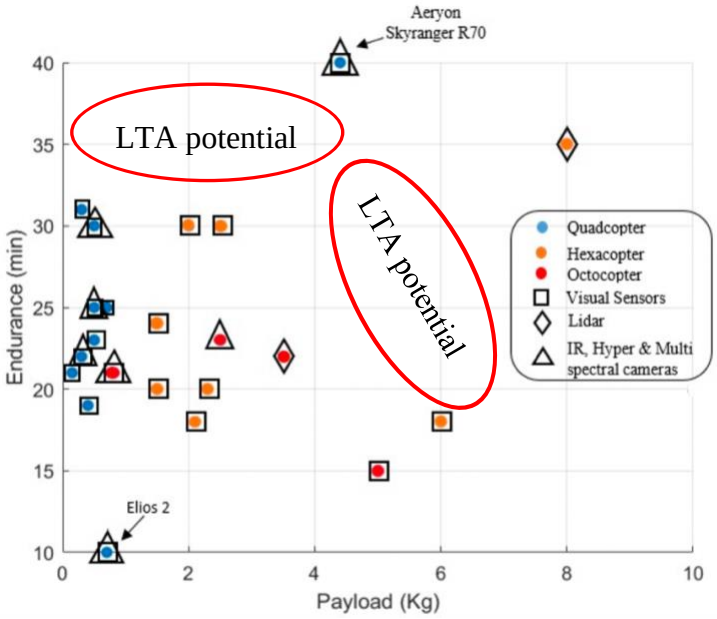

Fig. 6. Multicopter endurance vs payload chart. [35]

Airships and blimps are a subset of lighter-than-air drones and can offer solutions to some of the limitations of fixed-wing and multicopter aircraft. Blimps are composed of a cigar-shaped envelope filled with a lighter-than-air lifting gas such as hydrogen or helium and are controlled using motors and/or rudders. The first powered airship flight was in France in 1853 [53, p. 8]. By the 1920s, Germany was conducting regular transatlantic flights, but since the explosion of the *Hindenburg* in 1937, most commercial passenger transport has ceased [53, pp. 8–11]. The *Hindenburg* caught fire because it was filled with hydrogen, which is flammable [53, p. 11]. Despite this history, airships have distinct benefits as remote sensing platforms. Namely, LTA drones can have exceptional endurance and payload capabilities while being less expensive than manned aircraft [54]. The lift that keeps these airships aloft is dependent on the density of the lifting gas used and the volume of the envelope. The relationship between the amount of lift generated is demonstrated in [55, eq. (3)]:

$$L = V(\rho_A - \rho_G)g \tag{3}$$

where L is the lift force, V is the volume of gas enclosed by the envelope, g is the acceleration due to gravity, and ρ_A and ρ_G are the density of air and the lifting gas, respectively. If more payload is needed, more gas can be used [53, p. 109]. That means that nearly all the battery's energy can be used to propel the airship forward, like a fixed-wing. This allows large airships to remain aloft for many hours [53, p. 721]. But unlike a fixed-wing, airships have no minimum speed because the lift is not dependent on a wing moving through the air [53, p. 15],[54]. This allows for long flight durations with payloads only limited by the volume of lifting gas that can be held by the envelope.

Despite these advantages, there are some difficulties associated with the use of LTA drones for remote sensing including the lifting gases and inherent instability. The common lifting gases helium and hydrogen pose logistical problems. Helium is five to ten times more expensive than hydrogen and is a non-renewable resource [53, p. 313],[56]. Hydrogen can provide about 8% more lift than helium because it is less dense. However, hydrogen is extremely flammable while helium is an inert gas [53, p. 47].

Airships exhibit an inherent instability that can be attributed to aerodynamic instability and the Munk moment. A diagram of common blimp axes is provided in [57]. The aerodynamic center of an airship is the point where the pitch or yaw moments do not depend on pitch or yaw angle [53, p. 74]. Airships are usually directionally unstable in the yaw axis because the aerodynamic center (a.c.) is forward of the center of gravity (c.g.) as seen in [53, p. 276, Fig. 7].

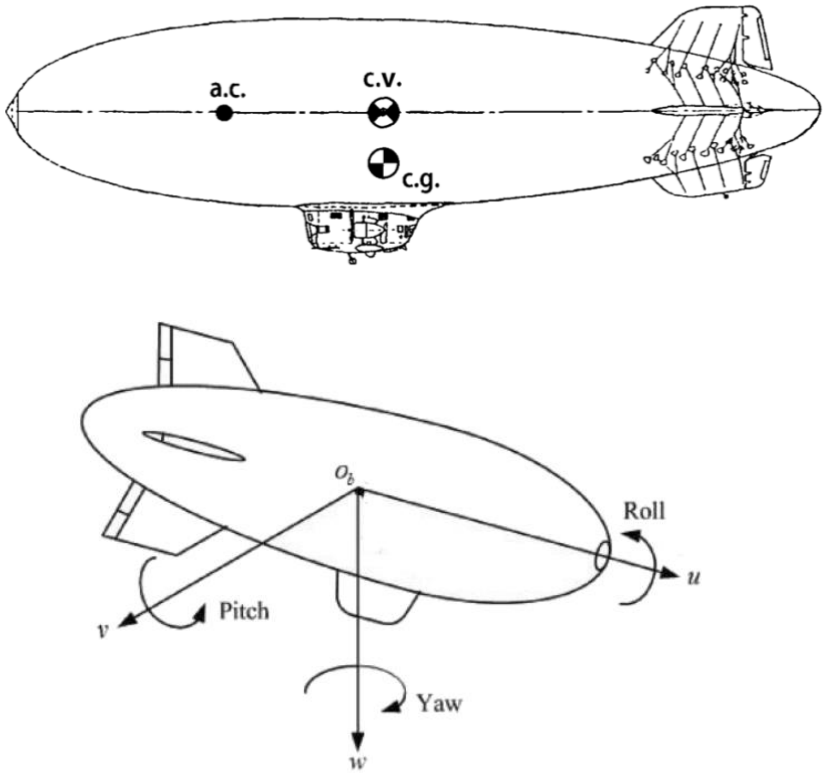

Fig. 7. Diagram of an airship. [53, p. 276]

Even small yaw moments introduced by small external forces can introduce an acceleration about the yaw axis [53, p. 277]. The Munk moment destabilizes airships in pitch and yaw and is an example of this inherent instability. When an airship rotates about the pitch or yaw axis, the Munk moment tends to turn the airship perpendicular to the direction of flow. This is because the pressure is highest on the front of the airship and lowest on the back [58]. These inherent instabilities mean that even the slightest wind gust or pilot input can initiate a pitch or yaw rate that will continue until it is arrested by the pilot or control system [53, p. 299]. Airships are more sensitive to gusts than other aircraft because they have a low mass-to-volume ratio. When an airship encounters a gust of wind, more momentum is transferred to the airship compared to other aircraft [59]. In most airships, the center of gravity lies beneath the center of volume (c.v.) which creates

a pendulum-like effect. Pitch axis instability is countered by a restoring torque caused by this pendulum [60],[61]. However, no such pendulum effect is present in the yaw axis. One approach to stabilizing the yaw axis is to increase the size of the airship's fins. However, the size of the fins needed to completely stabilize the airship is often too big for the airship's weight budget. This is because airships operate at low speeds, which means fins need to be large to be effective [59].

This inherent instability can be improved by increasing the envelope size or implementing active flight control. Active flight stabilization can address instability through closed-loop control. Changes in pitch, roll, and yaw are monitored by a flight controller which then continuously makes adjustments to control surfaces to maintain the airship's course [55],[62]. Increasing envelope size increases stability because both the mass and inertia of a rigid body oppose external forces and moments while in dynamic equilibrium. This relationship is established in [55, eq. (4), (5)] :

$$m\dot{\boldsymbol{v}} = \boldsymbol{F} \tag{4}$$

$$[I]\dot{\boldsymbol{\omega}} = \boldsymbol{T} \tag{5}$$

where m is the mass, $\boldsymbol{v}$ is the linear velocity, $\boldsymbol{F}$ is the sum of the external forces, $[I]$ is the inertia matrix, a $\boldsymbol{\omega}$ is the angular velocity, and $\boldsymbol{T}$ is the sum of the external torques.
If an airship has a larger mass and inertia, more external force or torque will be needed to produce a change in velocity. The effect of this property is increased by added mass and added inertia. Other aircraft types displace a mass of air that is insignificant compared to the mass of the vehicle. In contrast, the mass of air that an airship displaces must be considered because it is nearly equal to its mass [55]. The linear and angular momentum of the displaced air results in added mass and added inertia terms which further stabilize the airship [53, pp. 889–899]. A larger envelope will have more mass and inertia as well

as added mass and inertia which will help to stabilize the airship against external forces and moments. The destabilizing Munk moment will increase linearly with changes in envelope size, but the increasing moment of inertia will counteract this moment because it scales proportionally to the square of each increase in dimension [58]. This relationship is demonstrated in Fig. 8, where an ellipsoid is forced with an arbitrary loading case. The moment of inertia increases with length faster than the Munk moment, meaning that larger envelopes have greater resistance to this instability.

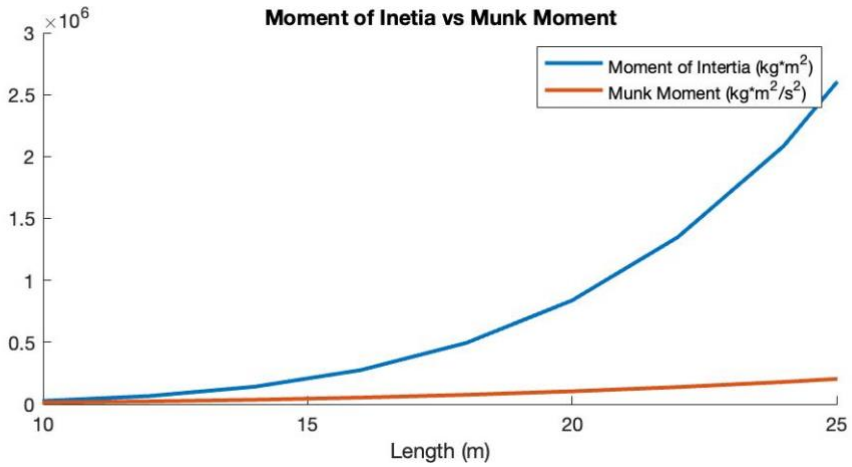

Fig. 8. Moment of Inertia vs Munk Moment.

The purpose of this work was to see how this remote-controlled blimp performed in the glacier research setting and to better understand the limitations of its use in this environment. The blimp's performance in the presence of wind and gusts was observed, and the flight stability was analyzed. The end goal was to assess how to improve this small-scale, aerial sensing platform so this lighter-than-air technology can be better utilized in future Earth Science research.

METHODS

Research program and test site

The assessment of this small-scale blimp for remote sensing research was conducted during participation in the Juneau Icefield Research Program (JIRP). JIRP is run primarily through the University of Maine's Climate Change Institute and School of Earth and Climate Sciences with support from the University of Alaska Southeast's Department of Environmental Science. The program involves a six-week, 120 km traverse of the Juneau Icefield and 10-14 day stays at the major field camps. While at these camps, the bulk of the scientific research is conducted by 35 students and 10-15 faculty and staff [63]. Blimp test flights were performed at the second field camp along the traverse, Camp 10, in the nearby North Basin from July 7th, 2021, to July 15th, 2021. A map of Camp 10's location and the test site is provided in Fig. 9.

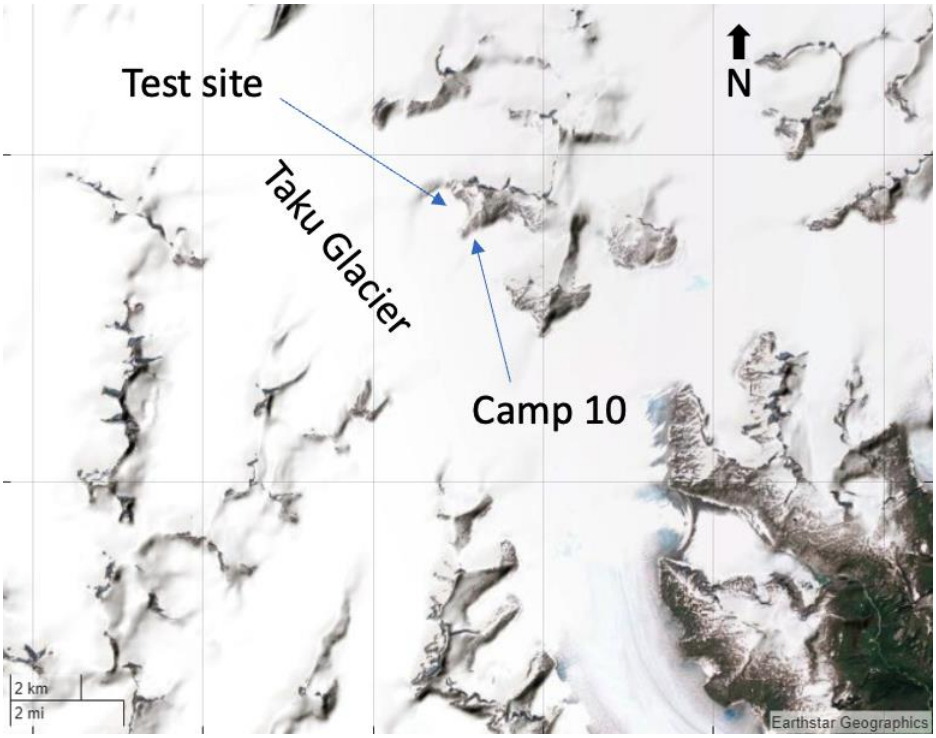

Fig. 9. Camp 10 and the North Basin test site.

Camp 10's North Basin was chosen for its low average summer wind speed, proximity to the camp, and potential for scientific research. Low wind speed was desired because of the small blimp's inherent wind sensitivity. Wind speed data from weather stations at camps 10, 17, and 18 showed median wind speeds of 1.8 m/s, 4.5 m/s, and 2.5 m/s respectively from June to August and from years 2013 to 2018 [64]. Relative to the other camps, Camp 10 had milder historical winds, which made it a favorable location for a blimp that had not yet been tested in winds. The North Basin is adjacent to the nunatak where Camp 10 is located, which made for easy access with personnel and equipment. Exposed bedrock outcroppings surround the basin, which provided locations for the study of bedrock fracture density and orientation. Photogrammetry could also be used to study subglacial lake volume changes which result in the rising or falling of the glacier ice surface on an annual basis as the lake fills and drains. The NASA Jet Propulsion Lab is considering the North Basin for testing an ice drill and sub-glacial lake water sampling instrumentation on future missions to Europa, so a better understanding of the subglacial hydrodynamics may be helpful to future research in the area [65].

Vehicle

The vehicle that was tested in this research was a 3.4 m long, remote-controlled (RC), airship that was purchased from Berlin Zeppelin, a German supplier, for about $700 USD [66]. The manufacturer advertised the flight time as one hour. The envelope was made from a proprietary synthetic material, the gondola and tail cone were made from hard plastic, and the fins are made of foam. The plastic and foam components were attached with Velcro to the envelope and the electronics were secured inside the gondola. The airship kit was marketed to RC LTA hobbyists, and it was designed to be flown

indoors. The necessary electronics included brushless motors, electronic speed controllers (ESCs), a servo, battery, radio receiver, radio transmitter, and a telemetry module. A diagram of these components is provided in Appendix A.

As seen in Fig. 10, thrust was provided by two motors on the side of the gondola which can rotate to control pitch using the servo. Yaw was controlled with a motor mounted on the tail cone. The envelope's volume was approximately 1.9 m^3 and was measured to produce a lift of 330 grams after the needed electrical components were installed. A diagram of these components is provided in Appendix A. In addition to the essential electrical components, GoPro sized multispectral camera and GPS were added to the bottom of the gondola to capture photos and flight data. A parts list including costs is provided in Appendix A. Fig. 11 shows the full assembly of the blimp pictured with the pilot as a size reference.

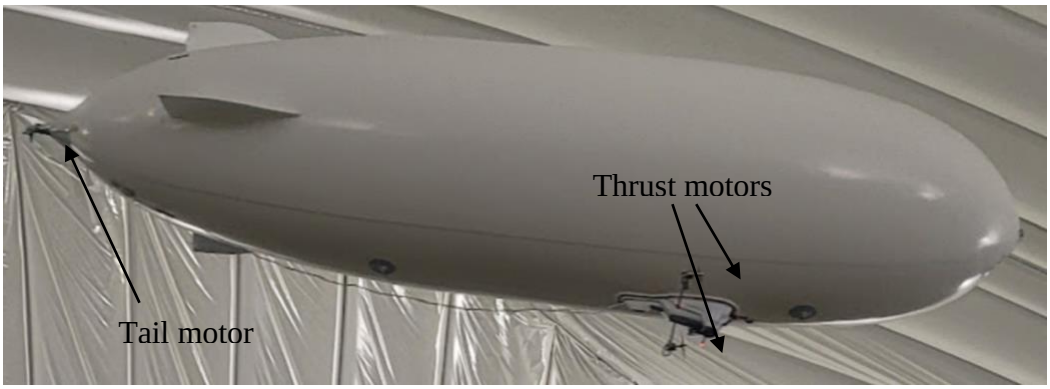

Fig. 10. A picture of the propulsion elements.

Fig. 11. The blimp shown ready for flight with pilot as a size reference.

The blimp kit from Berlin Zeppelin included all components needed to fly except for the electronic components. Electrical components were ordered based on recommendations by Berlin Zepplin. Once the electronic components were installed, an initial test flight was conducted in the Mahaney Sports Dome at the University of Maine, Orono campus in April 2021. No data was collected during this flight, but the remote-control systems were tested and were found to be operational. The airship demonstrated its ability to handle the payload of the multispectral camera and GPS unit, and directional instability was observed, but not quantified. Given the observed instability, the plan was made to test the blimp in little to no wind in Alaska, with the potential to fly in higher winds if good control could be maintained. With the flight systems in working order, the airship was packaged and sent to Juneau in early June 2021.

Testing Logistics

The logistics of the flight testing in Alaska were difficult but doable. The blimp and helium tanks were brought to Camp 10 on the Juneau Icefield by helicopter during a regular resupply flight to the camp. Helium was chosen as the lifting gas due to its inert

nature and safety. The rental of two 150 cubic foot helium tanks, and a pressure regulator for two months from a local industrial supplier, Tyler Rental, cost $792. This was enough gas for five fills of the blimp, but only one of these tanks was needed because the blimp was stored inflated when not in use. The airship was stored in a 10’x15’ portable garage tent that was purchased for $200 at the Juneau Home Depot, which was erected at the testing site in the bottom of the North Basin as seen in Fig. 12. Batteries were charged at Camp 10 when the camp’s generator was running and then brought into the North Basin for test flights. These flights required low wind and no precipitation. In the two weeks that the research group was at Camp 10, only two days met these good weather criteria: July 7th and July 15th, 2021.

Fig. 12. Blimp garage and storage location in the North Basin.

In these two days, five test flights were accomplished. A photograph of one of these flights is provided in Fig. 10. Before flight testing, a range test of the radio controller was performed to make sure that radio communication would not be lost while in the North Basin. This involved one researcher driving away on a snowmobile with the

controller, a GPS unit, and a walkie-talkie. Another researcher observed the blimp's motors and reported to the first researcher on the walkie-talkie. Control of the motors with no noticeable interruption or signal loss was maintained for 1.85 km, which was measured by the GPS. This test was terminated after 1.85 km because the snowmobile was too far away to see with the naked eye. It is likely that the effective range is over 1.85 km, which is larger than the North Basin which is 1.0 km across. Preparation for test flights involved topping off the helium in the garage and trimming the airship to ensure level flight. Also, washers were placed in pouches in the front and rear of the blimp until the blimp was level and barely negatively buoyant (~5g of negative buoyancy). This slight negative buoyancy prevented a sudden ascent if control of pitch was lost.

Fig. 13. Test flight in the North Basin

The goal of this testing was to understand the feasibility of this small-scale LTA drone for remote sensing. To accomplish this, the objectives for test flights were to a) test endurance, b) test the control and stability of the blimp in the research setting in low wind, c) acquire images of bedrock to test the usefulness of the platform for remote sensing, and d) test in higher wind conditions if good control could be maintained. The test site is exhibited in Fig. 13. Endurance was assessed by flying the drone until the

battery was 95% discharged and recording the flight time. This meant discharging 11.1V Lipo battery in the blimp from 12.6V to 10.83V. Control and stability were assessed qualitatively by the pilot who recorded ground airspeed, the approximate interval of time between course corrections, and notes on the flight. Stability was quantitatively assessed by deriving angular accelerations and variability in heading from the GPS data. The ability of the blimp to capture remote sensing data was assessed by comparing it with a DJI Phantom 4 Quadcopter in attempted photogrammetry missions.

All flights were performed in accordance with FAA P.L. 115-254, Section 350, Part 107 (14 CFR part 107), and 49 U.S.C. § 44809 regulatory framework [67]. These guidelines included but were not limited to flying within line of sight with a maximum altitude of 400 ft and operating in a safe and controlled manner.

Initial analysis of Alaska flight data

During the test flights in Alaska, various data types were collected including multispectral images, GPS points, observations, endurance times, and wind speeds. Endurance times were averaged to assess the flight time of the airship and pictures were post-processed to see if photogrammetry models could be made. A qualitative assessment of stability was made by averaging the approximate time between course corrections needed to maintain heading. Wind speeds and observations were compared with performance data to inform decisions about which data sets to use for comparison to dome flights. Although a detailed qualitative assessment was made of the blimp's performance, a quantitative basis was needed to design changes.

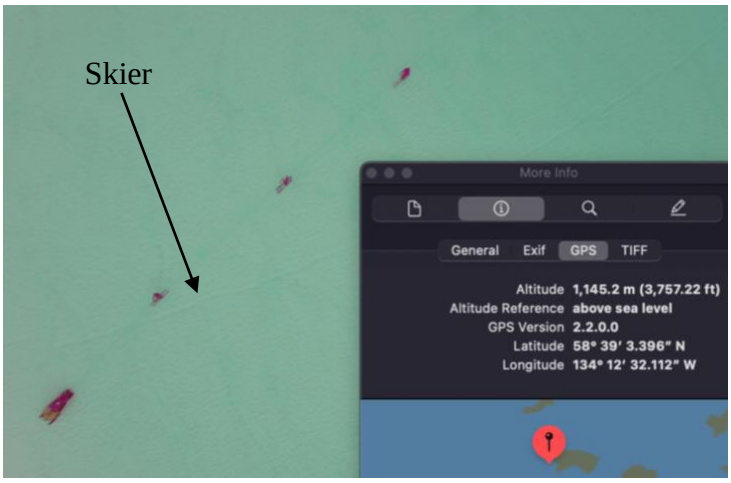

Fig. 14. An example multispectral photo with a GPS tag.

Out of the five test flights in Alaska, GPS data was collected throughout the entirety of two flights and in a portion of one of the flights. Photos were taken by the multispectral camera every three seconds. Each photo was tagged by the GPS with a time, latitude, longitude, and altitude, as seen in Fig 14. To remove the GPS data from the metadata of each photo, a command-line tool called ExifTool was used which stripped all the GPS data into a .csv file [68]. The latitude and longitude were reported by the GPS in degrees, and extraneous GPS points were filtered out of the datasets of each of the three flights where GPS was recorded. MATLAB's azimuth function was used to convert the latitude and longitude of each data point to a heading [69]. To convert a difference in degrees to a difference in meters a function that returns the Earth-Centered Earth-Fixed Cartesian offset between the geodetic coordinates was implemented in MATLAB [70]. This function returned the change in distance in the x, y, and z directions. The distance flown in three dimensions was then obtained by finding the Euclidean distance using nested hypotenuse functions. The code for this calculation is provided in [1].

Problem identification and modification

To assess whether the observed instability was in the yaw or pitch axis, angular accelerations were calculated. Larger accelerations were expected to correlate with less stable flight and smaller accelerations were expected in more stable flight. This is like aircraft turbulence, where less stable, more turbulent flight is characterized by higher accelerations. The second derivative of the headings was taken to determine angular acceleration in the yaw axis. Pitch angles between GPS points were obtained by taking the inverse sine of the z-axis offset over the incremental distance traveled in three dimensions. Angular acceleration in the pitch axis was found by taking the second derivative of these pitches with respect to time. Absolute value of ngular acceleration of both axes was plotted spatially to create a visualization of the rate of change in angular velocity as the blimp moved through the air. Based on these spatial representations, the blimp's performance could be assessed in different maneuvers such as straight flight, turns, ascent, and descent. Angular accelerations in the pitch axis and yaw axis were averaged across the entirety of the flight to see which axis was most unstable.

This comparison informed design decisions regarding the modification of the airship to improve its performance. First, modification options were assessed to address this instability. These options included larger fins, active flight control, gyro stabilization, a smaller tail motor, and a larger envelope. Next, a design decision was made, and the blimp was modified. The airship was retested in the Mahaney Sports Dome, to see if the change resulted in increased performance. Directional instability was assessed using a compass so that variability in heading could be compared with the variability in heading from the flights in Alaska. Instead of a GPS and camera, a Pixhawk flight controller with

an internal compass was installed in the blimp. A GPS was not used in the dome because the GPS could not connect to enough satellites to acquire a fix through the dome's ceiling. Also, endurance was not formally assessed in the dome because comparing flight times without assessing the distance traveled with GPS would lend little useful insight into changes in performance.

Comparing data after the modification

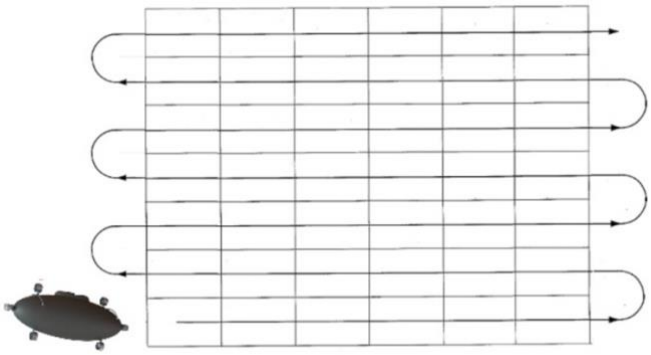

Fig. 15. Example of a flight path. [54]

The predominant instability in the Alaskan fights was in the yaw axis, so performance after modification was assessed as a function of variability in the heading. Angular acceleration provides information about how fast an aircraft turns, but heading variability shows how much an aircraft deviates from its course. In the research setting, a pilot often acquires an image set by flying long, straight transects over the target area in a grid-like pattern as shown in Fig 15 [54]. Most of the flight will be spent performing these transects so it is more relevant to compare how well an aircraft maintains its course rather than how well it turns. Thus, variability in heading was chosen over yaw axis acceleration because it is a more relevant measure of yaw axis instability. Heading

variability analysis was not performed in the pre-modification data processing because the yaw instability had not yet been identified as the primary issue.

Two flights with similar missions and conditions were compared to assess whether modification of the blimp improved heading variability. In the fifth flight on the Icefield, the goal was to fly straight to a bedrock outcropping and return. Fig. 16 shows the flight path of this flight. In the subsequent dome test, the goal was to maintain a straight flight for as long as possible to provide a realistic comparison. Both test flights were conducted in conditions of no wind. The data collected by the compass used in the dome sampled heading every 40 milliseconds. To make a significant comparison, the data from the dome was downsampled to the same rate as the Alaska flights, one point every three seconds.

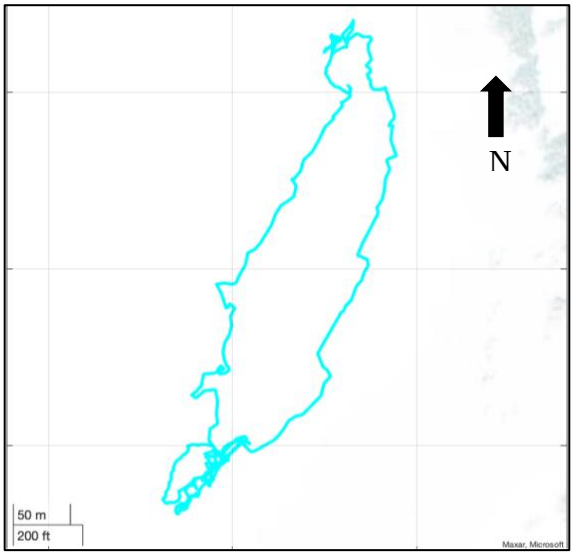

Fig. 16. Test flight #5 path.

Heading data may be unrealistically variable if pilot-initiated turns are compared with segments of straight flight, so these flight maneuvers needed to be separated. Assessing variation over the whole dataset would not accurately represent heading instability because this does not control for instances when the pilot changes the airship's

course. It is thus necessary that maneuvers are separated, and variability assessed within each maneuver. The final assessment of the performance in directional stability came from the median variability across each discrete flight maneuver, rather than from the continuous variability across the test.

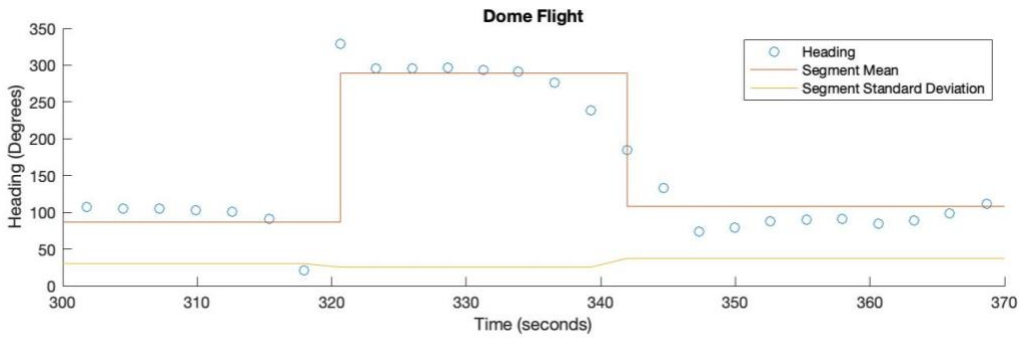

Fig. 17. An example of heading variance grouping.

Hand-picking these sections of flight would have resulted in selection bias and human error, so this grouping process was automated. The transition between straight flight and a turn is characterized by an abrupt change in heading. To automatically identify this, a MATLAB filter that finds abrupt changes in variance was used [71],[72]. The data were grouped into sections that have less than 20 degrees of variance in heading. This grouping is illustrated in an example of the results in Fig. 17. Thresholds of 5, 10, 20, 25, and 30 degrees of variance were also tested, but 20 degrees of variance did the best job of grouping turns and straight flight across both data sets. Thresholds over 20 degrees tended to underfit the data, while thresholds of under 20 degrees tended to overfit the data. The segments of straight flight with low standard deviation in heading were more stable than segments with high standard deviation. This grouping also allowed for the separate assessment of heading variability within a turn. More stable turns were characterized by low standard deviations and less stable turns had higher standard

deviations. To see if the modifications to the blimp addressed the instability, the median standard deviation of all flight segments was compared between test flights in Alaska and in the dome.

Statistical uncertainty and hypothesis testing

The statistical uncertainty of this comparison was also addressed. Statistical significance needed to be quantified as different sensors were used, and the data came from different populations. It is common practice to address the uncertainty in experimental data collected with a digital measuring device by equating the uncertainty to the smallest increment of the sensor [73]. The GPS used in Alaska had an uncertainty of $\pm 1 \times 10^{-8}$ degrees in latitude and longitude. In contrast, the compass used in the dome had an uncertainty of ± 0.01 degrees in heading. The effect of these GPS uncertainties on mean angular acceleration calculations was $\pm 0.34\%$. This was assessed in accordance with American Society of Mechanical Engineers guidelines for measurement uncertainty PTC 19.1, as it allows for the simple estimation of uncertainty through multistep processes [74]. The same method was used to assess experimental uncertainties in the median heading variance across the flights. The compass and GPS uncertainty had a negligible effect on the median variance in Alaska and in the dome.

A confidence interval was used to test the statistical significance of whether a modification to the blimp was associated with a decrease in directional instability. The confidence interval was set at 99% and a left-tailed hypothesis test was performed. The null hypothesis was that the medians were the same, and the alternative hypothesis stated that the median of the dome flight variance was less than the median of Alaska flight variance. Because this data was not normally distributed, a Wilcoxon rank-sum test was

used which is recommended for comparing medians of independent non-parameterized data [75],[76],[77].

Uncertainty was also assessed in calculations of wind speed, course correction, and endurance. A Kestrel Weather Meter was used to measure ground wind speed which had a $\pm$ 0.1 mph or $\pm$ 0.04 m/s uncertainty, again using the smallest increment of the device as the error. The digital watch that was used to approximate intervals between course correction reported to the nearest second, so the accuracy was assumed to be $\pm$ 1 second. The same watch was used to measure endurance, but only the nearest minute was recorded. Thus, the uncertainty for each endurance measurement is $\pm$ 1 minute. The Kline and McClintock equations were used to propagate this uncertainty through calculations of average wind speed, course correction, and endurance [73]. The code for these calculations is presented in [1].

RESULTS AND DISCUSSION

Results from the flights in Alaska

The average endurance throughout the flights in Alaska was 32 $\pm$ 1 minute. This was shorter than the one-hour flight time which was predicted by the manufacturer, but it was longer than the 25-minute endurance observed in the DJI Phantom 4 Pro+ which carried the same multispectral camera as payload. Even during flights with no wind, the maximum endurance was 37 $\pm$ 1 minutes. This means that the difference between expected flight time and average flight time cannot be completely attributed to the presence of wind. Endurance was shown to decrease with increasing wind speed as seen in Fig. 18. This could be a result of two factors: more energy was used by the thrust motor to fly against the wind and/or more energy was used by the tail motor to correct for instabilities in the yaw axis.

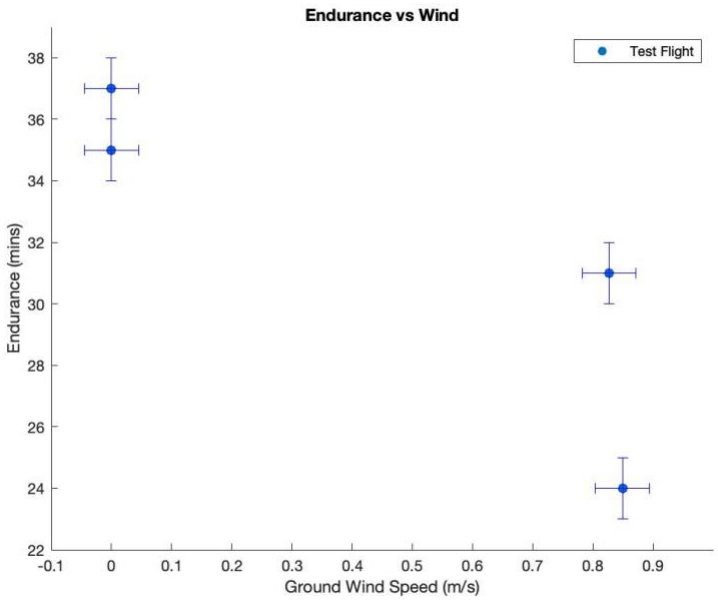

Fig. 18. The effect of wind on endurance.

While the blimp had a longer endurance than the Phantom 4 drone, it did not have better usability in the presence of wind. The pilot reported difficulty maintaining heading while flying upwind. Even in low winds of less than 1 m/s, the blimp was challenging to maintain stable control, and the test flight was terminated. These reports are detailed in the flight logs in Appendix B. In comparison, the Phantom 4 Pro+ is stable in the presence of winds up to 10 m/s [78]. This difference in wind resistance is likely due to the Phantom 4's active flight stabilization and the blimp's smaller mass-to-volume ratio which tends to make airships more sensitive to wind than smaller aircraft [59]. The average interval between course corrections needed to maintain heading was 3 ± 1 seconds. Fig. 19 demonstrates that the pilot needed to steer more frequently on flights with more wind.

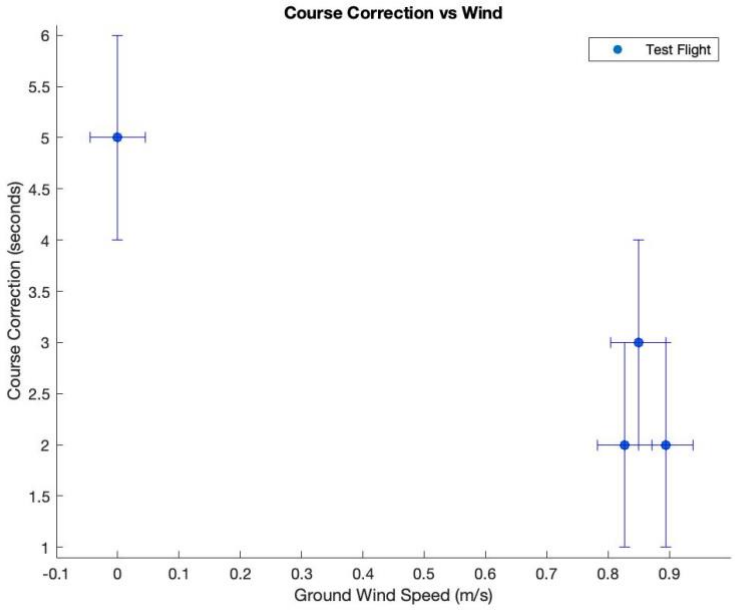

Fig. 19. The effect of wind on course correction.

Compared to the blimp, the Phantom 4 was also easier to use for glacier research because the logistics were simpler, and it was easier to control. The pre-flight setup of the

blimp which included topping off helium and trimming ballast, took anywhere from 15 to 30 minutes. Whereas the quadcopter setup, which only included attaching propellers, took less than one minute. The blimp was also less mobile than the Phantom 4. The airship needed to be stored in its garage when not in use, while the case that housed the quadcopter could be placed in a backpack and be brought to any research site. To change research sites with the blimp, a helicopter or snowmobile would need to be used to relocate the garage and helium tanks. The Phantom 4 needed no manual pitch or yaw control and completed several research missions in a range of weather conditions. In contrast, even on flights with no wind, the blimp needed manual course corrections every 5 ± 1 seconds to maintain its course. Difficulty controlling the elevation was also noted in the flight logs provided in Appendix B. Due to these challenges, the blimp could not be controlled well enough to methodically image bedrock outcroppings. It was flown slowly enough to gather detailed photographs, but the pilot was unable to coordinate the imaging of areas of interest.

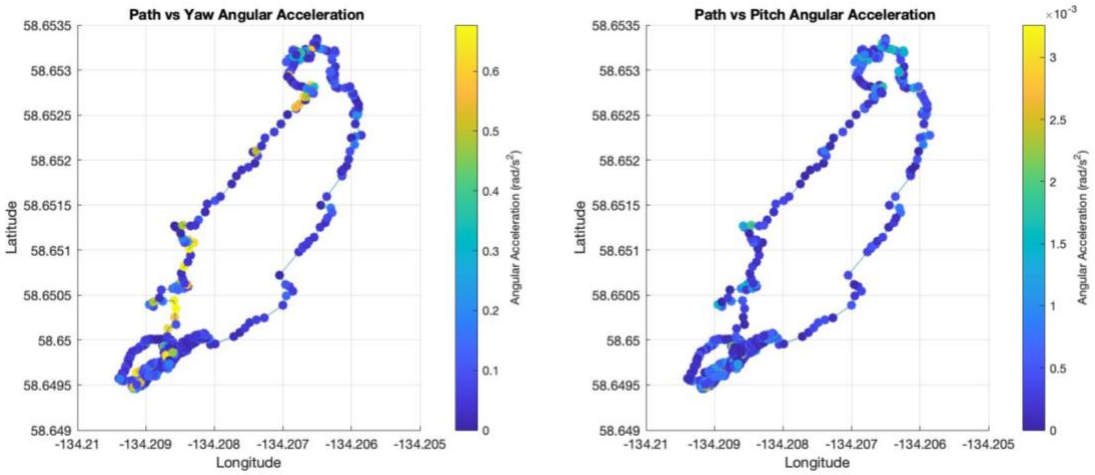

Fig. 20. Yaw vs pitch angular accelerations.

To better understand the difficulty in yaw and pitch control that was observed in Alaska the GPS data was processed to derive angular accelerations which were plotted

spatially. This analysis was done on test flight five because no wind was present. Therefore, the effect of wind did not complicate this analysis. As seen in Fig. 20, large yaw accelerations were observed even in portions of relatively straight flight. This pattern was thought to be characteristic of instability in the yaw axis. Large accelerations were not present in the same sections of flight in the pitch axis, which helped to constrain the primary instability to the yaw axis. Furthermore, the average pitch angular acceleration was $5.31 \times 10^{-4}\ \frac{rad}{s^2}$ while the average pitch angular acceleration was $1.28 \times 10^{-1}\ \frac{rad}{s^2}$. Yaw angular acceleration was $243 \pm .34\%$ times greater than pitch angular acceleration which suggests that instability was greater in the yaw axis than in the pitch axis.

Too much stability results in an aircraft with too little maneuverability, but too little stability results in an aircraft that does not keep its course. These data point towards instability in the yaw axis as the primary difficulty in control because the most obvious symptom was the blimp's inability to maintain a steady heading. These observations are supported in the physics of small airships. The small envelope size made this airship sensitive to wind and prone to instability [53, pp. 889–899]. Also, the Munk moment and aerodynamic instability destabilized the yaw axis more than the pitch axis because the center of gravity was beneath the center of mass [58], [53, p. 276].

Modification

After the yaw axis instability was identified as the airship's primary instability, a range of modification options were assessed. However, before assessing these options, a theory was developed about how to improve the airship's ability to maintain its course. This theory was used to inform the modification which was associated with a performance benefit. A component of the yaw instability was suspected to be inherent to

the blimp and its physical properties. This inherent instability was thought to be exacerbated by oversteer from an oversized tail motor. The blimp's natural tendency to change heading required the pilot to make frequent course corrections using the tail motor. However, if the tail motor was too powerful, even slight inputs would cause oversteer. Larger fins had the potential to stabilize the yaw axis, but the size of fins needed was likely too large [59]. Active flight control was effective in stabilizing the Phantom 4, but its complexity was beyond the scope of this project. The option of gyroscopic stabilization was explored, but the stabilizers currently on the market were not able to handle the magnitude of angular accelerations that were observed. The concept of a larger envelope was promising but increasing the size of the envelope did not address the oversteer problem as directly or as simply as a reduction in the thrust output of the tail motor. Reducing the size of the tail motor was settled on, and this change was expected to improve performance by limiting the effects of inherent directional instability.

As seen in Fig. 21, a new motor and propeller combination was selected based on what components were freely available at UMaine's Crosby Lab. The motor and propeller that were used in the Alaska testing were calculated to produce 1,289 g of thrust at maximum throttle. The smaller motor and propeller combination was calculated to produce 520 g of thrust at full throttle, a 59% reduction in output. These calculations are presented in Appendix C and were performed using the software ECalc, the industry standard for RC performance calculations [79].

Fig. 21. The larger motor compared with the smaller motor.

Results from the dome flight

After the smaller tail motor was installed, a single test flight in the Mahaney Sports Dome was performed. The pilot noted improvements in usability and ability to maintain heading. Yaw rates were arrested with a small reversal of the tail rotor after a turn, and the large changes in heading that were characteristic of flights in Alaska were reduced. While precise start and end times were not recorded, an endurance was estimated as over one hour. This improvement in endurance could be a result of less reliance on an overpowered tail motor or because the flight in the dome was slower than in Alaska.

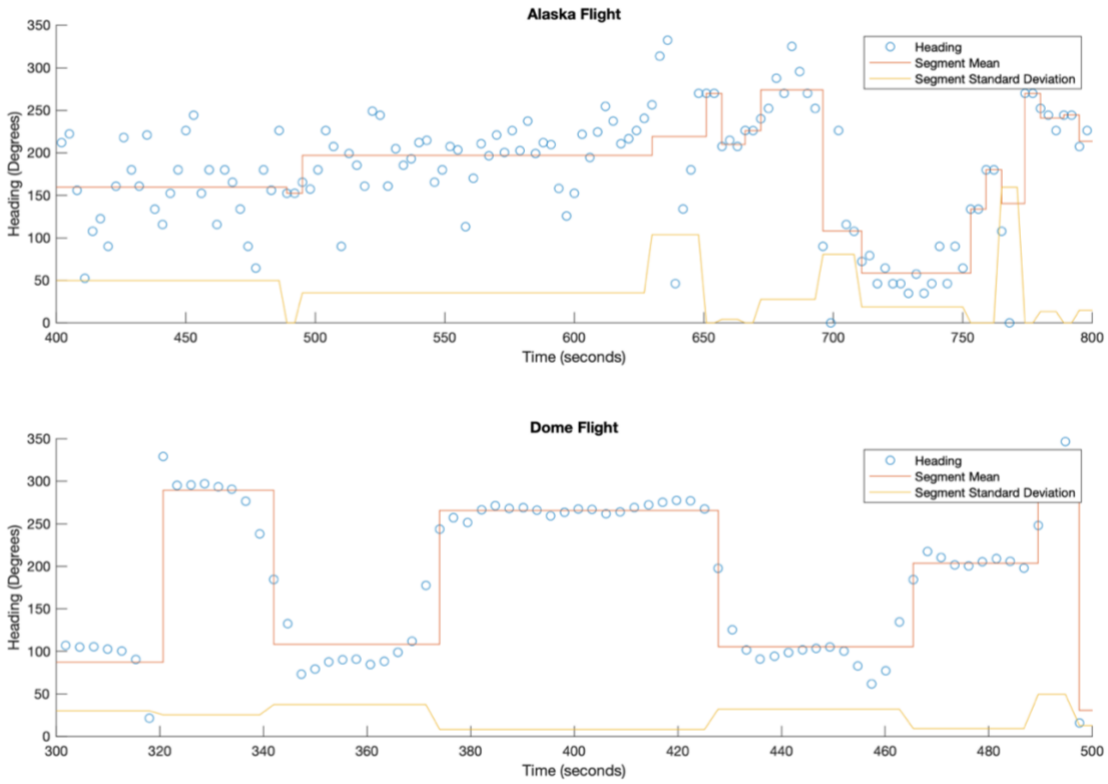

Fig. 22. Heading comparison between flights in Alaska and the dome.

These qualitative assessments were substantiated with heading data collected by the onboard compass. A comparison in the heading data is shown in Fig 22. The data were segmented into groups that have less than 20 degrees of variance in heading. The segments of straight flight with low standard deviation in heading were more stable than segments with high standard deviation. The top plot likely shows more variability between sections of straight flight because the effects of inherent yaw instability were greater in Alaska. In the bottom plot, there is a large decrease in standard deviation because the heading is less variable across sections of flight. The median heading standard deviation decreased by 47% across flight segments between the two groups. This decrease suggests that flight was more stable after the tail motor was reduced, but the statistical significance of this comparison needed to be assessed.

The confidence interval was set at 99% and a left-tailed hypothesis test was performed. The null hypothesis that the medians were the same was rejected in favor of the alternative hypothesis that the median of the dome flight variance was less than the median of Alaska flight variance. This test had a p-score of 1.11×10^{-10} which allowed for a high degree of certainty in the statistical significance of the hypothesis test. It is nearly certain that the heading variance was reduced between the Alaska flights and the dome flights. The high statistical certainty in this comparison was attributed to the large sample size, how far apart the medians were, and the high precision of the experimental data.

Limitations

Some confounding variables were not controlled which limited the results of this research. The angular accelerations that were used to identify yaw instability were also dependent on pilot oversteer; however, without data on the pilot input this effect is unknown. Additionally, these accelerations were dependent on GPS data with a coarse, three-second temporal resolution. The microclimate in the North Basin where the testing occurred was also not accounted for. Temperature and pressure gradients caused by the differential heating between warm bedrock and cold snow may have affected the blimp. Observations on differences in performance near these features at different elevations remain unresolved. Lastly, the Munk moment increases with velocity, and this effect was not incorporated into the stability analysis [58]. For example, the improvements observed after modification to the blimp may not be a result of the reduction in tail motor, but rather a reduction in flight speed. While the statistical uncertainty associated with the hypothesis testing in this research was low, there is considerable uncertainty in the

experimental design because of the inability to control these variables. While multiple associations were established in this research, no cause-and-effect relationships was concluded. If these factors were better controlled for, causality could have been determined.

CONCLUSIONS AND FUTURE WORK

Conclusions

This research was conducted from February 2021 to April 2022. It involved modifying a small-scale blimp using off-the-shelf components in the spring of 2021 and bringing it to the Juneau Icefield to test in a novel research setting that summer. In the fall, the flight data was processed to inform the modification that was tested in the spring of 2022. The performance of the blimp in Alaska was assessed qualitatively and quantitatively to show that improvements to the blimp were made.

The blimp did not work well for its mission of collecting data on bedrock fracture density and orientation in Alaska. The primary reason for this was that it was difficult to manually control and too sensitive to wind to acquire useful image sets. Because the blimp could not be safely controlled in winds greater than 0.89 ± 0.04 m/s, there were only two days with mild enough weather on the Icefield for flights to be made. Transportation and setup of the blimp were also cumbersome and time-consuming. In comparison, a DJI Phantom 4 Pro+ quadcopter was used to study bedrock outcroppings in place of the blimp. It efficiently collected data in variable wind conditions and was easy to pilot.

Nonetheless, there were promising findings for the future of lighter-than-air technology in Earth Science research. The blimp had better endurance than the DJI Phantom with the same payload. The logistics of flying a blimp in the polar research setting were challenging but certainly feasible. Also, the blimp was shown to move slowly enough to capture detailed images, while supporting an adequate payload for long flights. After the blimp was modified, there were considerable improvements in handling.

Future work

The learning experiences of this work have prompted interesting avenues for future work. Using similar methods, researchers could examine the effect of airship velocity on instability. Furthermore, active flight control could make collecting data with blimps as easy as flying an actively stabilized drone. Once active stabilization is achieved, the transition to autonomous flight through waypoints and flight planning can be made. This would allow for more efficient data collection over longer spatial and temporal spans than is possible with remote-controlled flight. Larger envelopes may also provide better lift and stability than smaller envelopes, so envelope size optimization analysis could help determine the minimum size needed to maintain these benefits.

REFERENCES

[1] M. Burtis, *LTA_thesis*. 2022. Accessed: Apr. 02, 2022. [Online]. Available: https://github.com/maxburtis/LTA_thesis

[2] J. R. Jensen, *Remote sensing of the environment: an earth resource perspective*, 2nd ed. Upper Saddle River, NJ: Pearson Prentice Hall, 2007.

[3] S. I. Jiménez-Jiménez, W. Ojeda-Bustamante, M. de J. Marcial-Pablo, and J. Enciso, "Digital Terrain Models Generated with Low-Cost UAV Photogrammetry: Methodology and Accuracy," *ISPRS Int. J. Geo-Inf.*, vol. 10, no. 5, Art. no. 5, May 2021, doi: 10.3390/ijgi10050285.

[4] M. J. Westoby, J. Brasington, N. F. Glasser, M. J. Hambrey, and J. M. Reynolds, "'Structure-from-Motion' photogrammetry: A low-cost, effective tool for geoscience applications," *Geomorphology*, vol. 179, pp. 300–314, Dec. 2012, doi: 10.1016/j.geomorph.2012.08.021.

[5] J. Baqersad, P. Poozesh, C. Niezrecki, and P. Avitabile, "Photogrammetry and optical methods in structural dynamics – A review," *Mech. Syst. Signal Process.*, vol. 86, pp. 17–34, Mar. 2017, doi: 10.1016/j.ymssp.2016.02.011.

[6] "Agisoft Metashape." https://www.agisoft.com/ (accessed Mar. 24, 2022).

[7] "Structure from motion photogrammetry in physical geography - M.W. Smith, J.L. Carrivick, D.J. Quincey, 2016." https://journals-sagepub-com.wv-o-ursus-proxy02.ursus.maine.edu/doi/full/10.1177/0309133315615805?utm_source=summon&utm_medium=discovery-provider (accessed Mar. 24, 2022).

[8] H. Zhang, E. Aldana-Jague, F. Clapuyt, F. Wilken, F. Clapuyt, and V. Oost, "Evaluating the Potential of PPK Direct Georeferencing for UAV-SfM Photogrammetry and Surface Change Detection," p. 33.

[9] L. Inzerillo, "INTEGRATED SFM TECHNIQUES USING DATA SET FROM GOOGLE EARTH 3D MODEL AND FROM STREET LEVEL," p. 7, 2017.

[10] G. Roberti *et al.*, "Structure from motion used to revive archived aerial photographs for geomorphological analysis: an example from Mount Meager volcano, British Columbia, Canada," *Can. J. Earth Sci.*, vol. 58, no. 12, pp. 1253–1267, Mar. 2021, doi: 10.1139/cjes-2020-0140.

[11] A. Keutterling and A. Thomas, "Monitoring glacier elevation and volume changes with digital photogrammetry and GIS at Gepatschferner glacier, Austria," *Int. J. Remote Sens.*, vol. 27, no. 19, pp. 4371–4380, Oct. 2006, doi: 10.1080/01431160600851819.

[12] J. L. Chen, C. R. Wilson, and B. D. Tapley, “Contribution of ice sheet and mountain glacier melt to recent sea level rise,” *Nat. Geosci.*, vol. 6, no. 7, Art. no. 7, Jul. 2013, doi: 10.1038/ngeo1829.

[13] Z. Zuo and J. Oerlemans, “Contribution of glacier melt to sea-level rise since AD 1865: a regionally differentiated calculation,” *Clim. Dyn.*, vol. 13, no. 12, pp. 835–845, Dec. 1997, doi: 10.1007/s003820050200.

[14] S. O’Neel, E. Hood, A. L. Bidlack, S. W. Fleming, M. L. Arimitsu, and A. Arendt, “Icefield-to-Ocean Linkages across the Northern Pacific Coastal Temperate Rainforest Ecosystem,” *BioScience*, vol. 65, no. 5, pp. 499–512, 2015.

[15] W. Sun *et al.*, “Gravity measurements in southeastern Alaska reveal negative gravity rate of change caused by glacial isostatic adjustment,” *J. Geophys. Res. Solid Earth*, vol. 115, no. B12, 2010, doi: 10.1029/2009JB007194.

[16] C. F. Larsen, E. Burgess, A. A. Arendt, S. O’Neel, A. J. Johnson, and C. Kienholz, “Surface melt dominates Alaska glacier mass balance,” *Geophys. Res. Lett.*, vol. 42, no. 14, pp. 5902–5908, 2015, doi: 10.1002/2015GL064349.

[17] F. A. Ziemen *et al.*, “Modeling the evolution of the Juneau Icefield between 1971 and 2100 using the Parallel Ice Sheet Model (PISM),” *J. Glaciol.*, vol. 62, no. 231, pp. 199–214, Feb. 2016, doi: 10.1017/JOG.2016.13.

[18] Geosciences and E. C. S. Center, “Location of the Juneau Icefield,” 2017.

[19] D. J. Barclay, G. C. Wiles, and P. E. Calkin, “Holocene glacier fluctuations in Alaska,” *Quat. Sci. Rev.*, vol. 28, no. 21, pp. 2034–2048, Oct. 2009, doi: 10.1016/j.quascirev.2009.01.016.

[20] C. McNeil *et al.*, “Explaining mass balance and retreat dichotomies at Taku and Lemon Creek Glaciers, Alaska,” *J. Glaciol.*, vol. 66, no. 258, pp. 530–542, Aug. 2020, doi: 10.1017/jog.2020.22.

[21] R. Hugonnet *et al.*, “Accelerated global glacier mass loss in the early twenty-first century,” *Nature*, vol. 592, no. 7856, pp. 726–731, Apr. 2021, doi: 10.1038/s41586-021-03436-z.

[22] S. J. Cook, D. A. Swift, M. P. Kirkbride, P. G. Knight, and R. I. Waller, “The empirical basis for modelling glacial erosion rates,” *Nat. Commun.*, vol. 759, no. 11, 2020.

[23] R. A. DiBase, M. W. Rossi, and A. B. Neely, “Fracture density and grain size controls on the relief structure of bedrock landscapes,” *Geology*, vol. 46, no. 5, pp. 399–402, 2018.

[24] M. Dühnforth, R. S. Anderson, D. Ward, and G. M. Stock, “Bedrock fracture control of glacial erosion processes and rates,” *Geology*, vol. 38, no. 5, pp. 423–426, May 2010, doi: 10.1130/G30576.1.

[25] T. P. Lane, D. H. Roberts, B. R. Rea, C. O. Cofaigh, and A. Vieli, “Controls on bedrock bedform development beneath the Uummannaq Ice Stream onset zone, West Greenland,” *Geomorphology*, vol. 231, pp. 301–313, 2015.

[26] R. B. Alley, K. M. Cuffey, and L. K. Zoet, “Glacial erosion: status and outlook,” *Ann. Glaciol.*, vol. 60, no. 80, pp. 1–13, Dec. 2019, doi: 10.1017/aog.2019.38.

[27] N. Bursztyn, J. L. Pederson, C. Tressler, R. D. Mackley, and K. J. Mitchell, “Rock strength along a fluvial transect of the Colorado Plateau – quantifying a fundamental control on geomorphology,” *Earth Planet. Sci. Lett.*, vol. 429, pp. 90–100, Nov. 2015, doi: 10.1016/j.epsl.2015.07.042.

[28] B. A. Clarke and D. W. Burbank, “Quantifying bedrock-fracture patterns within the shallow subsurface: Implications for rock mass strength, bedrock landslides, and erodibility,” *J. Geophys. Res.*, vol. 116, no. F4, p. F04009, Oct. 2011, doi: 10.1029/2011JF001987.

[29] D. N. Scott and E. E. Wohl, “Bedrock fracture influences on geomorphic process and form across process domains and scales,” *Earth Surf. Process. Landf.*, vol. 44, no. 1, pp. 27–45, 2019, doi: 10.1002/esp.4473.

[30] S. G. Roy, G. E. Tucker, P. O. Koons, S. M. Smith, and P. Upton, “A fault runs through it: Modeling the influence of rock strength and grain-size distribution in a fault-damaged landscape,” *J. Geophys. Res. Earth Surf.*, vol. 121, no. 10, pp. 1911–1930, 2016, doi: 10.1002/2015JF003662.

[31] D. A. Brew and R. P. Morrell, “Intrusive rocks and plutonic belts of southeastern A laska, U.S.A.,” p. 24.

[32] H. Harris, “Artist, Icefield to Ocean. [Art]. JIRP.” 2021.

[33] D. Digitalcommons@umaine and C. Rand, “Estimating Bedrock Fracture Density of the Juneau Icefield, AK, to Inform Glacial Erosion Models,” 2020. [Online]. Available: https://digitalcommons.library.umaine.edu/honors

[34] “Drones to venture into Fukushima containment vessels - World Nuclear News.” https://www.world-nuclear-news.org/Articles/Drones-to-venture-into-Fukushima-containment-vesse (accessed Mar. 24, 2022).

[35] Z. Ameli, Y. Aremanda, W. A. Friess, and E. N. Landis, “Impact of UAV Hardware Options on Bridge Inspection Mission Capabilities,” *Drones*, vol. 6, no. 3, Art. no. 3, Mar. 2022, doi: 10.3390/drones6030064.

[36] B. P. Fitzpatrick, “UNMANNED AERIAL SYSTEMS FOR SURVEYING AND MAPPING: COST COMPARISON OF UAS VERSUS TRADITIONAL METHODS OF DATA ACQUISITION,” p. 52.

[37] “Are UAS More Cost Effective than Manned Flights?,” *Association for Unmanned Vehicle Systems International*, Oct. 24, 2013. https://www.auvsi.org/are-uas-more-cost-effective-manned-flights (accessed Mar. 24, 2022).

[38] “Amazon.com: DJI Phantom 4 Professional+ Quadcopter (Includes Display) CP.PT.000549 : Toys & Games.” https://www.amazon.com/DJI-Phantom-Professional-Quadcopter-CP-PT-000549/dp/B01N639RIJ (accessed Mar. 26, 2022).

[39] A. Jackman, “Consumer drone evolutions: trends, spaces, temporalities, threats,” *Def. Secur. Anal.*, vol. 35, no. 4, pp. 362–383, Oct. 2019, doi: 10.1080/14751798.2019.1675934.

[40] N. Barrera, Ed., *Unmanned aerial vehicles*. New York: Nova Science Publishers, 2021.

[41] “clarity-from-above-pwc.pdf.” Accessed: Apr. 05, 2022. [Online]. Available: https://www.pwc.pl/pl/pdf/clarity-from-above-pwc.pdf

[42] L. Kapustina, N. Izakova, E. Makovkina, and M. Khmelkov, “The global drone market: main development trends,” *SHS Web Conf.*, vol. 129, p. 11004, 2021, doi: 10.1051/shsconf/202112911004.

[43] “Consumer Drone Market Size Analysis | Industry Report, 2024.” https://www.grandviewresearch.com/industry-analysis/consumer-drone-market (accessed Apr. 06, 2022).

[44] H. González-Jorge, J. Martínez-Sánchez, M. Bueno, and A. P. Arias, “Unmanned Aerial Systems for Civil Applications: A Review,” *Drones*, vol. 1, no. 1, Art. no. 1, Dec. 2017, doi: 10.3390/drones1010002.

[45] “phx2.JPG (1129×543).” https://www.dronenerds.com/media/wysiwyg/phx2.JPG (accessed Apr. 06, 2022).

[46] “p4pv2-promotion-b4e0380818eeba7b93b25f110e2379cc.png (1418×720).” https://www2.djicdn.com/assets/images/products/phantom-4-pro/promotion/p4pv2-promotion-b4e0380818eeba7b93b25f110e2379cc.png?from=cdnMap (accessed Apr. 06, 2022).

[47] “vtol-drone.jpg (800×450).” https://s3-ap-southeast-1.amazonaws.com/assets.skyfilabs.com/images/blog/vtol-drone.jpg (accessed Apr. 06, 2022).

[48] "Physics_of_Flight.pdf." Accessed: Apr. 05, 2022. [Online]. Available: https://vsgc.odu.edu/geoted-uas/wp-content/uploads/sites/13/2019/09/Physics_of_Flight.pdf

[49] D. A. Flores, C. Saito, J. A. Paredes, and F. Trujillano, "Aerial photography for 3D reconstruction in the Peruvian Highlands through a fixed-wing UAV system," in *2017 IEEE International Conference on Mechatronics (ICM)*, Feb. 2017, pp. 388–392. doi: 10.1109/ICMECH.2017.7921137.

[50] "Lift Formula." https://www.grc.nasa.gov/www/k-12/WindTunnel/Activities/lift_formula.html (accessed Mar. 24, 2022).

[51] L. Roth, A. Hund, and H. Aasen, "PhenoFly Planning Tool: flight planning for high-resolution optical remote sensing with unmanned areal systems," *Plant Methods*, vol. 14, no. 1, p. 116, Dec. 2018, doi: 10.1186/s13007-018-0376-6.

[52] M. Honarmand and H. Shahriari, "Geological Mapping Using Drone-Based Photogrammetry: An Application for Exploration of Vein-Type Cu Mineralization," *Minerals*, vol. 11, no. 6, Art. no. 6, Jun. 2021, doi: 10.3390/min11060585.

[53] L. M. Nicolai, G. Carichner, and L. M. Nicolai, *Fundamentals of aircraft and airship design*. Reston, VA: American Institute of Aeronautics and Astronautics, 2010.

[54] P. Gili, M. Civera, R. Roy, and C. Surace, "An Unmanned Lighter-Than-Air Platform for Large Scale Land Monitoring," *Remote Sens.*, vol. 13, no. 13, p. 2523, Jun. 2021, doi: 10.3390/rs13132523.

[55] J. B. Mueller, M. A. Paluszek, and Y. Zhao, "Development of an Aerodynamic Model and Control Law Design for a High Altitude Airship," p. 18.

[56] G. Brumfiel, "The World Is Constantly Running Out Of Helium. Here's Why It Matters.," *NPR*, Nov. 08, 2019. Accessed: Mar. 26, 2022. [Online]. Available: https://www.npr.org/2019/11/01/775554343/the-world-is-constantly-running-out-of-helium-heres-why-it-matters

[57] W. Zhou, P. Zhou, Y. Wang, N. Wang, and D. Duan, "Station-keeping Control of an Underactuated Stratospheric Airship," *Int. J. Fuzzy Syst.*, vol. 21, no. 3, pp. 715–732, Apr. 2019, doi: 10.1007/s40815-018-0566-4.

[58] M. S. Triantafyllou and F. S. Hover, "MANEUVERING AND CONTROL OF MARINE VEHICLES".

[59] S. Suvarna, H. Chung, and R. S. Pant, "Design Methodology of a Small Unmanned Airship with Optimized Fins," in *2019 International Conference on*

Unmanned Aircraft Systems (ICUAS), Jun. 2019, pp. 1136–1142. doi: 10.1109/ICUAS.2019.8797920.

[60] S. B. V. Gomes, "An investigation into the flight dynamics of airships with application to the yez-2a," Ph.D., Cranfield University (United Kingdom), England. Accessed: Mar. 27, 2022. [Online]. Available: https://www.proquest.com/docview/301525209?https://www.library.umaine.edu/auth/EZProxy/test/authej.asp?url=parentSessionId=uxZwVTzx1lPI0fF9oa9ABep6AHbZuXNbLfVtnI4Gejo%3D&accountid=14583

[61] A. Kornienko, "System identification approach for determining flight dynamical characteristics of an airship from flight data," *Identifizierung der flugdynamischen Eigenschaften eines Luftschiffes aus Flugmessdaten*, 2006, doi: 10.18419/opus-3731.

[62] J. Raul Azinheira *et al.*, "Lateral/directional control for an autonomous, unmanned airship," *Aircr. Eng. Aerosp. Technol.*, vol. 73, no. 5, pp. 453–459, Oct. 2001, doi: 10.1108/EUM0000000005880.

[63] "The Icefield Traverse," *Juneau Icefield Research Program*. https://juneauicefield.org/icefield-traverse (accessed Mar. 28, 2022).

[64] E. H. Baker, S. McGee, S. W. Campbell, J. L. Pierce, and C. J. Mcneil, "Weather Station Data on the Juneau Icefield." U.S. Geological Survey, 2019. doi: 10.5066/P9DUI71J.

[65] Dr. Seth Campbell, JIRP Director, "Feedback on CUGR Proposal," Feb. 24, 2021.

[66] "Zeppelin-Bausatz für Modellbauer. Die Hülle ist bereits fertig verarbeitet!," *Berlinzeppelin, aufblasbare Werbedisplays aus der Hauptstadt*. https://www.berlinzeppelin.de/zeppelin-bausatz/ (accessed Apr. 05, 2022).

[67] "Educational Users." https://www.faa.gov/uas/educational_users/ (accessed Apr. 07, 2022).

[68] "ExifTool by Phil Harvey." https://exiftool.org/ (accessed Mar. 30, 2022).

[69] "Azimuth between points on sphere or ellipsoid - MATLAB azimuth." https://www.mathworks.com/help/map/ref/azimuth.html (accessed Mar. 30, 2022).

[70] "Cartesian ECEF offset between geodetic coordinates - MATLAB ecefOffset." https://www.mathworks.com/help/map/ref/ecefoffset.html (accessed Mar. 30, 2022).

[71] "Find abrupt changes in data - MATLAB ischange." https://www.mathworks.com/help/matlab/ref/ischange.html (accessed Mar. 30, 2022).

[72] R. Killick, P. Fearnhead, and I. A. Eckley, “Optimal detection of changepoints with a linear computational cost,” *J. Am. Stat. Assoc.*, vol. 107, no. 500, pp. 1590–1598, Dec. 2012, doi: 10.1080/01621459.2012.737745.

[73] “Errors-SFs-Uncertainties.pdf.” Accessed: Mar. 31, 2022. [Online]. Available: http://nebula2.deanza.edu/~lanasheridan/4A/Errors-SFs-Uncertainties.pdf

[74] “Citeseer - Full Text PDF.” Accessed: Apr. 08, 2022. [Online]. Available: http://citeseerx.ist.psu.edu/viewdoc/download;jsessionid=956364C5FDD521C8742555DF02042357?doi=10.1.1.820.7387&rep=rep1&type=pdf

[75] “Wilcoxon rank sum test - MATLAB ranksum.” https://www.mathworks.com/help/stats/ranksum.html (accessed Mar. 30, 2022).

[76] J. D. Gibbons and S. Chakraborti, *Nonparametric statistical inference*, 4th ed., rev.Expanded. New York: Marcel Dekker, 2003.

[77] “Nonparametric Statistical Methods. Myles Hollander and Douglas A. Wolfe, Wiley, Chichester, 1999. No. of pages: xiii+779. Price: £ 39.95. ISBN 0-471-19045-4 - Tiit - 2000 - Statistics in Medicine - Wiley Online Library.” https://onlinelibrary-wiley-com.wv-o-ursus-proxy02.ursus.maine.edu/doi/abs/10.1002/(SICI)1097-0258(20000530)19:10%3C1386::AID-SIM463%3E3.0.CO;2-X (accessed Mar. 30, 2022).

[78] “Phantom_4_Disclaimer_and_Safety_Guidelines_v1.2_en_160317.pdf.” Accessed: Apr. 01, 2022. [Online]. Available: https://dl.djicdn.com/downloads/phantom_4/en/Phantom_4_Disclaimer_and_Safety_Guidelines_v1.2_en_160317.pdf

[79] “eCalc - propCalc - the most reliable Propeller Calculator on the Web.” https://www.ecalc.ch/motorcalc.php (accessed Apr. 05, 2022)

[80] A. Paterson, C. Oxley, D. Bunker, and D. Ritger, “MEE 487 Detailed Design Report-Airships 1,” 2021.

APPENDICIES

APPENDIX A: BLIMP COMPONENTS

Component Name	Quantity	Manufacturer	Subtotal	Line Total
DX8 Transmitter	1	Spektrum	$400	$400
Servo	1	Generic	$10	~$10
Thrust ESC (20A)	2	QWinOut	$9	$9
Reversible ESC (20A)	1	Readytosky	$17	$17
2200 MaH 11.1V Lipo	1	Generic	$26	~$26
AR6600T Receiver	1	Spektrum	$65	$65
Tail Motor 2040 2280KV	1	Surpass Hobby		
Thrust Motor CF2822	2	EMax	$9	$18
Tail Prop 115mmx125mm 2-blade	1	Generic	$3	~$3
Thrust Prop APC06040	2	Horizon Hobby	$3	$6
Wires/connectors	n/a	Misc.	$20	~$20
Blimp Kit BZ320	1	Berlin Zeppelin	~$700	~$700
				~$1270

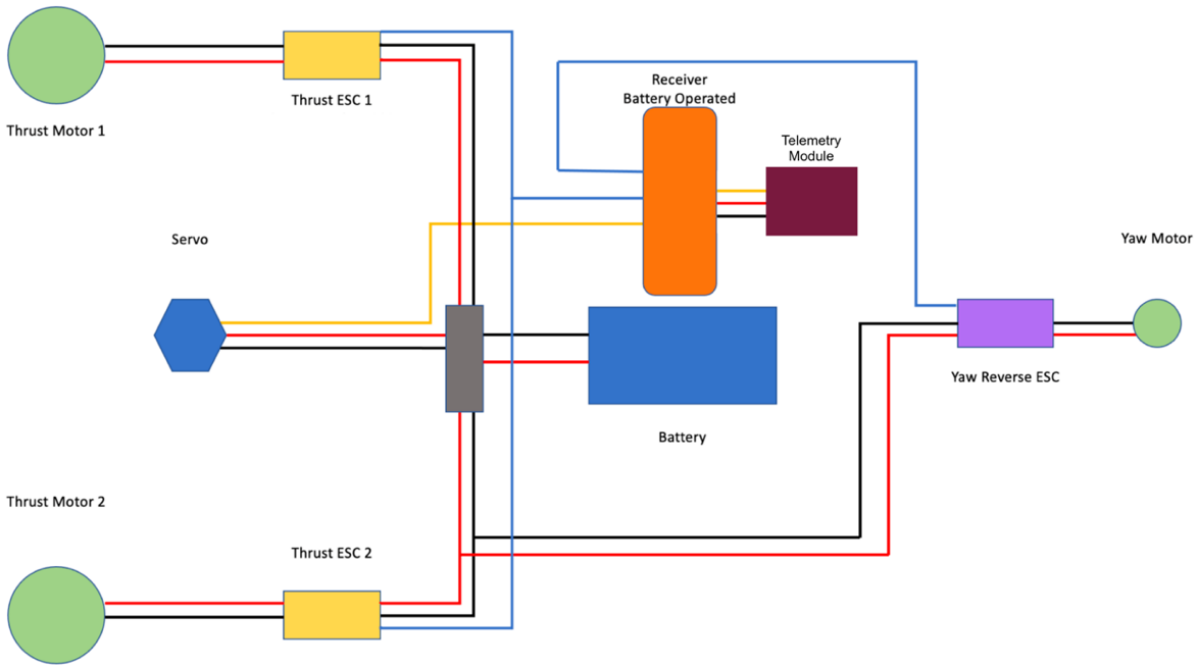

Wiring diagram of the electrical components. [80]

APPENDIX B: FLIGHT LOGS

Logs from Flights in Alaska

Windspeed and air temperature measurements were taken using a Kestrel Mini Weather Station immediately prior to the start of the flight.

Test Flight 1: 7/7/21

Takeoff: 9:30 AM	Date: 7/7/21	Ground Temp: 65°F
Landing: 9:40 AM	Vi: 12.2 V	Ground Airspeed: 2.0 mph
Time in Air: 10 mins	Vf: 11.3 V	Course correction: 2s

Notes:

- GOAL: Perform range test and perform a shake down flight to see what problems arise.
- Range test performed by driving away with the deflated blimp in a snowmobile across the glacier, communicating via radio with a stationary controller operator. Control of motors with no noticeable interruption or signal loss was maintained for 1.15 miles within line of sight. The test was terminated after 1.15 miles because the snowmobile was too far away to see with the naked eye. It is likely that the effective range is over 1.15 miles.
- 900 psi used to fill blimp.
- For the first flight, the blimp was loaded with ~20g of extra ballast above neutral buoyancy, a conservative measure to prevent uncontrolled floating upward.
- Blimp was landed before the battery ran out due to concern for decreased control as a result of increasing winds.
- No camera was used for this initial test flight so that it was not in risk of damage.
- Course correction (tail rotor use) to maintain course during flight occurred every 2s on average.

Test Flight 2:

Takeoff: 9:42 AM	Date: 7/15/21	Ground Temp: 55°F
Landing: 10:16 AM	Vi: 12.3 V	Ground Airspeed: 1.85 mph
Time in Air: 31 mins	Vf: 10.8 V	Course correction: 2s

Notes:

- GOAL: The focus of this test was endurance and to test camera.
- 100 psi was used to reinflate blimp after sitting for 8 days.
- Enough ballast was used to get the blimp barely negatively buoyant.
- Wind was catching on either side of the bow when flying against the wind, pulling the blimp to either side when flying against the wind, making it difficult to beat upwind.
- Running downwind was much more stable, and easier to maintain course.
- The camera and gps module were attached resulting in good trim but ~10g too much ballast (above neutral buoyancy).

- Between 9:43 and 9:46 the blimp was landed to start the interval timer on the camera.
- At one point when flying at a higher elevation, the blimp became positively buoyant, and the motors needed to be pointed downwards to prevent runaway ascent. The blimp returned to negative buoyancy upon descent.
- Upon landing at 10.8V, it was observed that one of the motors had rotated ~30 degrees downward, which likely contributed to the instability of the flight. This was fixed temporarily using electrical tape.
- Correction to maintain course during flight occurred every 2s on average.

Test Flight 3:

Takeoff: 10:57 AM	Date: 7/15/21	Ground Temp: 60°F
Landing: 11:34 AM	Vi: 12.3 V	Ground Airspeed: 0 mph
Time in Air: 37 mins	Vf: 10.7 V	Course correction: 5s

Notes:

- GOAL: The focus of this test was to repeat the endurance test and to continue testing camera.
- The increase in temperature during the day resulted in near perfect buoyancy, ~2-5g above neutral buoyancy.
- There was far better control and stability compared to previous flights, potentially because of there being no surface wind.
- As the blimp was flown away from the surface, positive buoyancy was observed, and the blimp needed to be flown downwards. This could be a result of changes in temperature and pressure at different elevations above the glacier.
- Correction to maintain course during flight occurred every 5s on average.
- No photos taken during this flight.

Test Flight 4:

Takeoff: 12:27 PM	Date: 7/15/21	Ground Temp: 66°F
Landing: 12:51 PM	Vi: 12.3 V	Ground Airspeed: 1.9 mph
Time in Air: 24 mins	Vf: 10.8 V	Course correction: 3s

Notes:

- GOAL: The focus of this test was to repeat the endurance test and use the camera to image a bedrock outcropping.
- To offset the increase in lift from the increasing ambient temperature, a washer was added to the tail to create negative buoyancy.
- This washer made the tail heavy, causing the blimp to be pointed slightly upward, which resulted in it tracking to higher elevations.
- To combat this, the blimp was flown slightly down during the ~50% of the flight.
- It was difficult to the orientation of the blimp in the distance, which way it was pointing with the white snowy backdrop.

- Better stability was maintained than in the first two flights, but it wasn't as stable as the previous flight.
- Upon reviewing the images, the camera stopped recording at some point before reaching the outcropping for an unknown reason.
- Correction to maintain course during flight occurred every 3s on average.

Test Flight 5:

Takeoff: 10:16 PM	Date: 7/15/21	Ground Temp: 50°F
Landing: 10:51 PM	Vi: 12.3 V	Ground Airspeed: 0 mph
Time in Air: 35 mins	Vf: 10.9 V	Course correction: 5s

Notes:

- GOAL: The focus of this test was to repeat the endurance test and use the camera to image a bedrock outcropping.
- It was hard to see the orientation of the blimp in the low light conditions
- There was serious instability observed as the blimp approached the bedrock outcropping including unexpected ascending. This instability was resolved when the blimp was flown near the surface of the snow at lower elevations.
- Upon reviewing the images, the camera did not pick up on any of the bedrock features because of the low light conditions with no direct sunlight.
- Correction to maintain course during flight occurred every 5s on average.

Other notes:

- One of the motor mounts was broken during shipping from Maine to Alaska which was fixed by heat welding the 3D printed part with a soldering iron upon arrival at Camp 10
- Weather was a limiting factor for this research. Out of the two weeks spent at Camp 10, I only had weather windows to fly for two days. This is because it was either windy, rainy, or I was required to help with the expedition in another way and couldn't devote resources towards flying.
- Construction of shelter went well, taking only about 4.5 hours of work with three people. However, melting occurred around the outside of the shelter that required the anchors to be reset every 4-5 days.
- While at Camp 10 I soldered on a voltage sensor and set up telemetry to get both voltage and G-force data. G-force logging over time would have been ideal, but I couldn't get the RC controller to save this log on the SD card that I had.
- Future flight speed calculations could be made by relating the GPS data from the photos to the flight time.
- Due to logistical challenges, lighting challenges, hardware malfunction, serious flight instability, and limited weather windows, I was unable to get a solid image set of any bedrock outcroppings using the blimp. Acquiring similar image sets using a multicopter was done easily about a dozen times during the expedition.

- Three days before leaving Camp 10 the tail motor mount on the blimp was damaged in a storm that resulted in 25 mph gusts in North Basin where the blimp was stored in its shelter. It is likely that the wind cut underneath the sidewalls of the shelter in a melted-out area of near the snow surface and bashed the blimp against the walls of the shelter where it was anchored down. No other damage was observed.

Log from Dome Flight

Test 1:

Date: 3/4/22	Course correction: 10s

Notes:

- GOAL: Perform as many straight transects across the dome as possible to acquire data on effect of the smaller tail motor and perform preliminary testing of Pixhawk flight controller and its effects on yaw stability.
- A vast improvement in ease of flight and ability to maintain heading.
- Yaw rates can be arrested with a small reversal of the tail rotor after a turn.
- While start and end times were not recorded, an estimated endurance of over one hour was observed.
- The Pixhawk controlled fast yaw rates well but did not react to slow yaw drift.
- No GPS lock in the Dome.
- Correction to maintain course during flight occurred every 10s on average.
- Endurance likely over one hour

APPENDIX C: THRUST CALCULATIONS

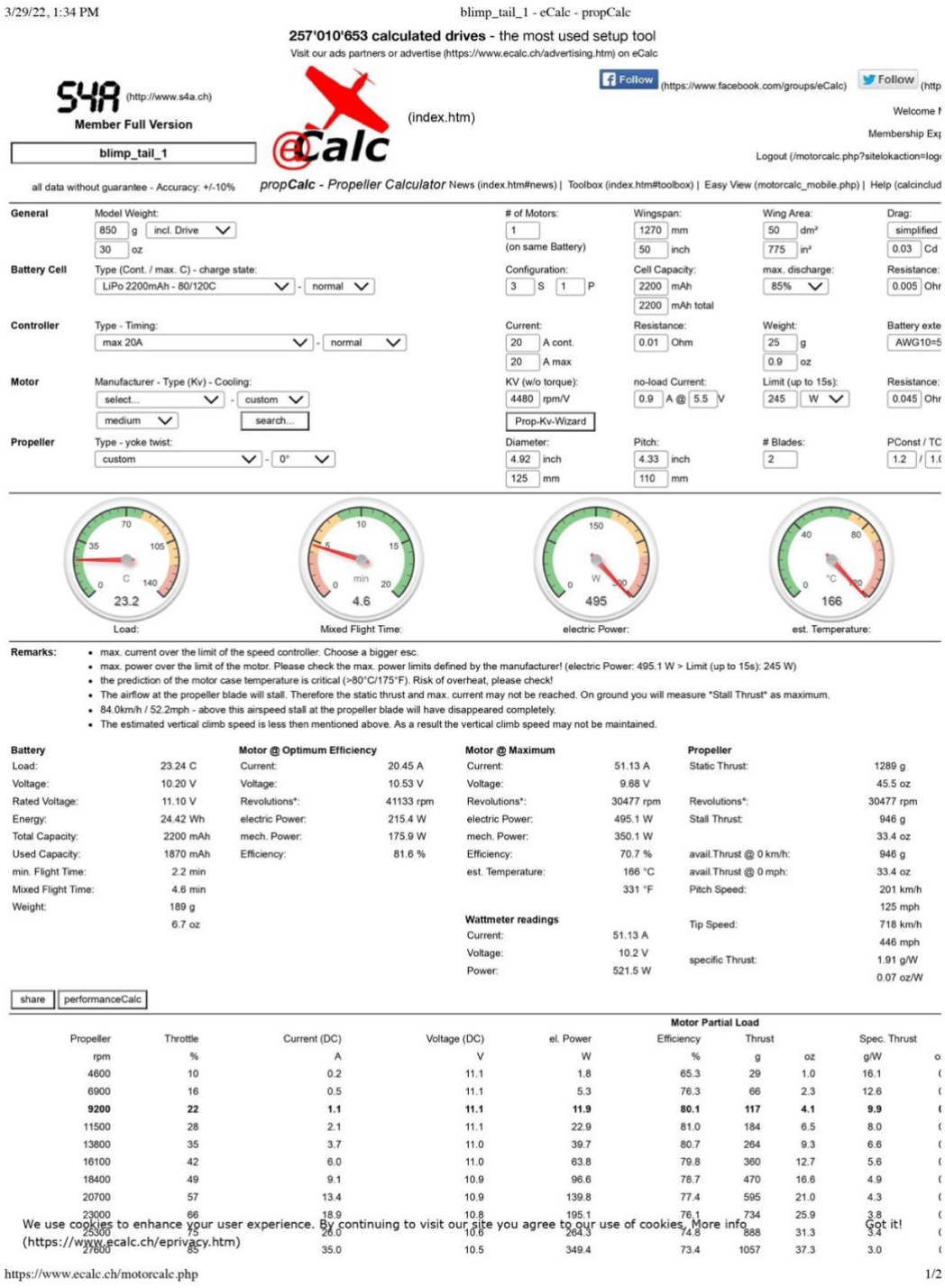

3/29/22, 1:34 PM blimp_tail_1 - eCalc - propCalc

257'010'653 calculated drives - the most used setup tool

Visit our ads partners or advertise (https://www.ecalc.ch/advertising.htm) on eCalc

S4A (http://www.s4a.ch) Member Full Version

eCalc (index.htm)

Follow (https://www.facebook.com/groups/eCalc) Follow (http

Welcome !

Membership Exp

Logout (/motorcalc.php?sitelokaction=log

blimp_tail_1

all data without guarantee - Accuracy: +/-10% *propCalc - Propeller Calculator* News (index.htm#news) | Toolbox (index.htm#toolbox) | Easy View (motorcalc_mobile.php) | Help (calcinclud

General	Model Weight: 850 g incl. Drive / 30 oz	# of Motors: 1 (on same Battery)	Wingspan: 1270 mm / 50 inch	Wing Area: 50 dm² / 775 in²	Drag: simplified 0.03 Cd	
Battery Cell	Type (Cont. / max. C) - charge state: LiPo 2200mAh - 80/120C - normal	Configuration: 3 S 1 P	Cell Capacity: 2200 mAh / 2200 mAh total	max. discharge: 85%	Resistance: 0.005 Ohr	
Controller	Type - Timing: max 20A - normal	Current: 20 A cont. / 20 A max	Resistance: 0.01 Ohm	Weight: 25 g / 0.9 oz	Battery exte AWG10=5	
Motor	Manufacturer - Type (Kv) - Cooling: select... - custom / medium / search...	KV (w/o torque): 4480 rpm / Prop-Kv-Wizard	no-load Current: 0.9 A @ 5.5 V	Limit (up to 15s): 245 W	Resistance: 0.045 Ohr	
Propeller	Type - yoke twist: custom - 0°	Diameter: 4.92 inch / 125 mm	Pitch: 4.33 inch / 110 mm	# Blades: 2	PConst / TC 1.2 / 1.(	

Load: Mixed Flight Time: electric Power: est. Temperature:

Remarks:

- max. current over the limit of the speed controller. Choose a bigger esc.
- max. power over the limit of the motor. Please check the max. power limits defined by the manufacturer! (electric Power: 495.1 W > Limit (up to 15s): 245 W)
- the prediction of the motor case temperature is critical (>80°C/175°F). Risk of overheat, please check!
- The airflow at the propeller blade will stall. Therefore the static thrust and max. current may not be reached. On ground you will measure *Stall Thrust* as maximum.
- 84.0km/h / 52.2mph - above this airspeed stall at the propeller blade will have disappeared completely.
- The estimated vertical climb speed is less then mentioned above. As a result the vertical climb speed may not be maintained.

Battery		**Motor @ Optimum Efficiency**		**Motor @ Maximum**		**Propeller**	
Load:	23.24 C	Current:	20.45 A	Current:	51.13 A	Static Thrust:	1289 g
Voltage:	10.20 V	Voltage:	10.53 V	Voltage:	9.68 V		45.5 oz
Rated Voltage:	11.10 V	Revolutions*:	41133 rpm	Revolutions*:	30477 rpm	Revolutions*:	30477 rpm
Energy:	24.42 Wh	electric Power:	215.4 W	electric Power:	495.1 W	Stall Thrust:	946 g
Total Capacity:	2200 mAh	mech. Power:	175.9 W	mech. Power:	350.1 W		33.4 oz
Used Capacity:	1870 mAh	Efficiency:	81.6 %	Efficiency:	70.7 %	avail.Thrust @ 0 km/h:	946 g
min. Flight Time:	2.2 min			est. Temperature:	166 °C	avail.Thrust @ 0 mph:	33.4 oz
Mixed Flight Time:	4.6 min				331 °F	Pitch Speed:	201 km/h
Weight:	189 g						125 mph
	6.7 oz			**Wattmeter readings**		Tip Speed:	718 km/h
				Current:	51.13 A		446 mph
				Voltage:	10.2 V	specific Thrust:	1.91 g/W
				Power:	521.5 W		0.07 oz/W

share performanceCalc

Motor Partial Load

Propeller	Throttle	Current (DC)	Voltage (DC)	el. Power	Efficiency	Thrust		Spec. Thrust	
rpm	%	A	V	W	%	g	oz	g/W	o
4600	10	0.2	11.1	1.8	65.3	29	1.0	16.1	(
6900	16	0.5	11.1	5.3	76.3	66	2.3	12.6	(
9200	**22**	**1.1**	**11.1**	**11.9**	**80.1**	**117**	**4.1**	**9.9**	**(**
11500	28	2.1	11.1	22.9	81.0	184	6.5	8.0	(
13800	35	3.7	11.0	39.7	80.7	264	9.3	6.6	(
16100	42	6.0	11.0	63.8	79.8	360	12.7	5.6	(
18400	49	9.1	10.9	96.6	78.7	470	16.6	4.9	(
20700	57	13.4	10.9	139.8	77.4	595	21.0	4.3	(
23000	66	18.9	10.8	195.1	76.1	734	25.9	3.8	(
25300	75	26.0	10.6	264.3	74.8	888	31.3	3.4	(
27600	85	35.0	10.5	349.4	73.4	1057	37.3	3.0	(

https://www.ecalc.ch/motorcalc.php 1/2

29900	96	46.3	10.3	452.4	72.1	1240	43.8	2.7	(
30477	100	51.1	10.2	495.1	70.7	1289	45.5	2.6	(

Motor Characteristic at Full Throttle

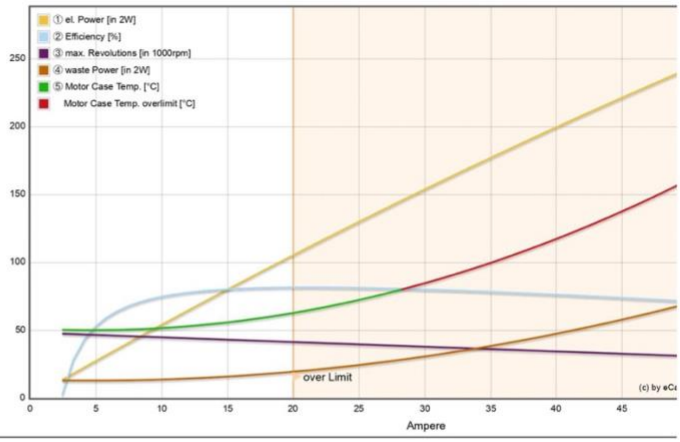

Important Note:
Before flight recheck your max. current! If your Current, el. Power or RPM are over the manufacturers limits your motor, controller and/or battery may take damage! **Verify before flight by measurment!**

*** *** ***

257'010'653 calculated drives - the most used setup tool

S4A (http://www.s4a.ch)

Member Full Version

eCalc (index.htm)

blimp_tail_2

all data without guarantee - Accuracy: +/-10%

propCalc - Propeller Calculator News (index.htm#news) | Toolbox (index.htm#toolbox) | Easy View (motorcalc_mobile.php) | Help (calcinclud

General	Model Weight: 850 g incl. Drive / 30 oz	# of Motors: 1 (on same Battery)	Wingspan: 1270 mm / 50 inch	Wing Area: 50 dm² / 775 in²	Drag: simplifi 0.03	
Battery Cell	Type (Cont. / max. C) - charge state: LiPo 2200mAh - 80/120C - normal	Configuration: 3 S 1 P	Cell Capacity: 2200 mAh / 2200 mAh total	max. discharge: 85%	Resistan 0.005	
Controller	Type - Timing: max 20A - normal	Current: 20 A cont. / 20 A max	Resistance: 0.01 Ohm	Weight: 25 g / 0.9 oz	Battery e AWG1	
Motor	Manufacturer - Type (Kv) - Cooling: iFlight - XING X1408 (3600) / medium / search...	KV (w/o torque): 3600 rpm/V / Prop-Kv-Wizard	no-load Current: 0.9 A @ 5.5 V	Limit (up to 15s): 245 W	Resistan 0.12	
Propeller	Type - yoke twist: custom - 0°	Diameter: 3 inch / 76.2 mm	Pitch: 5.6 inch / 142.2 mm	# Blades: 3	PConst / 1.2 /	

Load:

Mixed Flight Time:

electric Power:

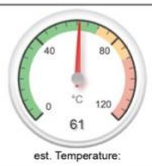

est. Temperature:

Remarks: • The airflow at the propeller blade will stall. Therefore the static thrust and max. current may not be reached. On ground you will measure *Stall Thrust* as maximum.

Battery		**Motor @ Optimum Efficiency**		**Motor @ Maximum**		**Propeller**	
Load:	5.59 C	Current:	12.33 A	Current:	12.29 A	Static Thrust:	520 g
Voltage:	10.88 V	Voltage:	10.76 V	Voltage:	10.76 V		18.3 oz
Rated Voltage:	11.10 V	Revolutions*:	31626 rpm	Revolutions*:	31646 rpm	Revolutions*:	31646 rpm
Energy:	24.42 Wh	electric Power:	132.6 W	electric Power:	132.3 W	Stall Thrust:	195 g
Total Capacity:	2200 mAh	mech. Power:	95.9 W	mech. Power:	95.6 W		6.9 oz
Used Capacity:	1870 mAh	Efficiency:	72.3 %	Efficiency:	72.3 %	avail.Thrust @ 0 km/h:	520 g
min. Flight Time:	9.1 min			est. Temperature:	61 °C	avail.Thrust @ 0 mph:	18.3 oz
Mixed Flight Time:	11.1 min				142 °F	Pitch Speed:	270 km/h
Weight:	189 g			**Wattmeter readings**			168 mph
	6.7 oz			Current:	12.29 A	Tip Speed:	455 km/h
				Voltage:	10.88 V		283 mph
				Power:	133.7 W	specific Thrust:	1.47 g/W
							0.05 oz/W

share performanceCalc

Motor Partial Load

Propeller	Throttle	Current (DC)	Voltage (DC)	el. Power	Efficiency	Thrust		Spec. Thrust	
rpm	%	A	V	W	%	g	oz	g/W	oz
4800	13	0.1	11.1	1.1	30.0	12	0.4	10.7	0
7200	20	0.2	11.1	2.4	47.1	27	0.9	11.2	0
9600	27	0.4	11.1	4.6	58.3	48	1.7	10.4	0
12000	34	0.7	11.1	8.0	65.3	75	2.6	9.4	0
14400	41	1.2	11.1	13.0	69.5	108	3.8	8.3	0
16800	48	1.8	11.1	19.9	72.0	146	5.2	7.4	0
19200	56	2.6	11.1	29.0	73.6	191	6.7	6.6	0
21600	64	3.7	11.0	40.8	74.5	242	8.5	5.9	0
24000	**72**	**5.1**	**11.0**	**55.6**	**75.0**	**299**	**10.5**	**5.4**	**0**
26400	**80**	**6.8**	**11.0**	**73.9**	**75.2**	**362**	**12.8**	**4.9**	**0**
28800	89	8.9	10.9	95.9	75.2	430	15.2	4.5	0
31200	98	11.3	10.9	122.1	75.1	505	17.8	4.1	0
31646	100	12.3	10.9	132.3	72.3	520	18.3	3.9	0

Motor Characteristic at Full Throttle

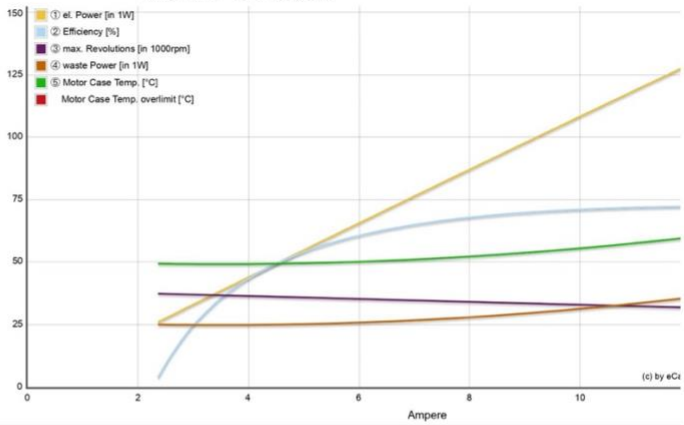

Important Note:
Before flight recheck your max. current! If your Current, el. Power or RPM are over the manufacturers limits your motor, controller and/or battery may take damage! **Verify before flight by measurment!**

AUTHOR'S BIOGRAPHY

Maxwell F. Burtis was born in Worcester, Massachusetts on November 20, 1999. He was raised in Brunswick, Maine, and graduated from Brunswick High School in 2018. Majoring in mechanical engineering, Maxwell has a minor in neuroscience. He is graduating as the Salutatorian of the 2022 graduating class. He is a member of the Sigma Phi Epsilon fraternity, the Senior Skull Honor Society, and is the president of the Pi Tau Sigma Mechanical Engineering Honor Society. After graduation, Max plans to manage his aquaculture company, Ferda Farms, while pursuing a master's degree in data science.